Injection of CO_2 with H_2S and SO_2 and Subsequent Mineral Trapping in Sandstone-Shale Formation

Tianfu Xu[1], John A. Apps[1], Karsten Pruess[1], and Hajime Yamamoto[2]

[1]Earth Sciences Division, Lawrence Berkeley National Laboratory, University of California, Berkeley, CA 94720, USA

[2]Civil Engineering Research Institute, Taisei Corporation, 344-1, Nase-cho, Totsuka-ku, Yokohama 245-0051, Japan

Abstract. Carbon dioxide (CO_2) injection into deep geologic formations can potentially reduce atmospheric emissions of greenhouse gases. Sequestering less-pure CO_2 waste streams (containing H_2S and/or SO_2) would be less expensive or would require less energy than separating CO_2 from flue gas or a coal gasification process. The long-term interaction of these injected acid gases with shale-confining layers of a sandstone injection zone has not been well investigated. We therefore have developed a conceptual model of injection of CO_2 with H_2S and/or SO_2 into a sandstone-shale sequence, using hydrogeologic properties and mineral compositions commonly encountered in Gulf Coast sediments of the United States. We have performed numerical simulations of a 1-D radial well region considering sandstone alone and a 2-D model using a sandstone-shale sequence under acid-gas injection conditions. Results indicate that shale plays a limited role in mineral alteration and sequestration of gases within a sandstone horizon for short time periods (10,000 years in present simulations). The co-injection of SO_2 results in different pH distribution, mineral alteration patterns, and CO_2 mineral sequestration than the co-injection of H_2S or injection of CO_2 alone. Simulations generate a zonal distribution of mineral alteration and formation of carbon and sulfur trapping minerals that depends on the pH distribution. The co-injection of SO_2 results in a larger and stronger acidified zone close to the well. Precipitation of carbon trapping minerals occurs within the higher pH regions beyond the acidified zones. In contrast, sulfur trapping minerals are stable at low pH ranges (below 5) within the front of the acidified zone. Corrosion and well abandonment due to the co-injection of SO_2 could be important

issues. Significant CO_2 is sequestered in ankerite and dawsonite, and some in siderite. The CO_2 mineral-trapping capability can reach 80 kg per cubic meter of medium. Most sulfur is trapped through alunite precipitation, although some is trapped by anhydrite precipitation and minor amount of pyrite. The addition of the acid gases and induced mineral alteration result in changes in porosity. The limited information currently available on the mineralogy of natural high-pressure acid-gas reservoirs is generally consistent with our simulations.

Key words. CO_2 sequestration, acid gas injection, mineral trapping, numerical simulation, Sandstone-shale sequence.

1. Introduction

A possible means of reducing carbon dioxide (CO_2) emissions to the atmosphere is through its injection into structural reservoirs in deep permeable geologic formations (Holloway, 1997). Such formations could include aquifers in sedimentary formations, structural traps in depleted oil and gas fields, and unmineable coal seams. Aquifers are, however, the most abundant fluid reservoirs in the subsurface and therefore the most promising structures for CO_2 injection. The deepest aquifers in the United States commonly contain brackish or saline water. Aquifers with salinities exceeding 10,000 mg/L total dissolved solids are excluded by the U.S. Environmental Protection Agency as underground sources of drinking water. Hence, they are logical targets for the eventual disposal of CO_2.

The feasibility of storing CO_2 in aquifers has been discussed in the technical literature over the last decade. Examples include an evaluation of the potential of CO_2 aquifer storage in The Netherlands (Lohuis, 1993) and in the Alberta Basin of Canada (Gunter et al., 1993, Bachu et al., 1994, Perkins and Gunter, 1995; Law and Bachu, 1996, Gunter et al., 1996 and 1997). Furthermore, large-scale CO_2 disposal in an aquifer is already being practiced in the Norwegian sector of the North Sea (Korbol and Kaddour, 1995). Recently, extensive experimental, field, and modeling studies of geological carbon sequestration have been conducted (Pearce et al., 1996; Rochelle et al., 1996; Gunter et al., 1997; Ortoleva et al., 1998; Johnson et al., 2001; White et al., 2001; McPherson and Lichtner, 2001; Oelkers et al., 2002; Knauss et al., 2002; Palandri and Kharaka, 2002; Strazisar and Zhu, 2002; Perkins et al, 2002; Pruess et al., 2003; Kaszuba, et al., 2003; Soong et al., 2004; Rosenbauer et al., 2005).

The sequestration of less-pure CO_2 waste streams (containing H_2S and/or SO_2) is less expensive or requires less energy to separate from flue gas or a coal gasification process streams, etc. Studies on injection of CO_2, together with H_2S and SO_2 have been reported recently. Knauss et al. (2002) presented the results of reactive transport simulations made to investigate the long-term impact of dissolved CO_2, H_2S and SO_2 on a sandstone formation. The results suggest that relatively high concentrations of H_2S in

CO_2 injection would not adversely impact injectivity or sequestration compared to the injection of CO_2 alone. The co-injection of SO_2, however, could produce significantly different results. In the long-term the simulations suggest that the formation of secondary carbonates could sequester a significant fraction of the injected CO_2, through the formation of calcite, magnesite and dawsonite.

Gunter et al. (2000) simulated the interaction of industrial waste streams comprising CO_2 and H_2S with the minerals in typical carbonate and sandstone aquifers from the Alberta Basin, Canada. The results support the idea that these acids can be neutralized by such reactions and that new mineral products are formed, such as calcite, siderite, anhydrite/gypsum and pyrrhotite. Siliciclastic aquifers appear to be a better host for "mineral trapping" than carbonate aquifers, especially with regard to CO_2.

Injection of CO_2 and H_2S derived from production of natural gas has been conducted in western Canada (Bachu et al., 2003). By the end of 2002, a total of approximately 40 acid-gas injection operations were active. Close to 1.5 Mt CO_2 and 1 Mt H_2S have been successfully injected into deep hydrocarbon reservoirs and saline aquifers in Canada alone. Approximately 16 acid-gas injection facilities are operating in the United States. These indicate that acid-gas injection is a mature and safe technology that can be applied elsewhere in the world. Furthermore, these acid-gas injection operations are analogous to future large-scale CO_2 geological sequestration to reduce CO_2 emissions into the atmosphere from large CO_2 point sources.

Numerical modeling of geochemical processes is necessary to investigate long-term injection of acid gases in deep aquifers, because aluminosilicate mineral alteration is very slow under ambient deep-aquifer conditions and is not amenable to experimental study. Xu et al. (2003) performed reactive transport simulations of CO_2 injection in a 1-D radial well region to analyze CO_2 immobilization through carbonate precipitation, under conditions representative of Gulf Coast sandstones of the Frio formation of Texas. Xu et al. (2004a) present a geochemical modeling analysis of the interaction of aqueous solutions under high CO_2 partial pressures with three different rock types. The first rock is a glauconitic sandstone from the Alberta Sedimentary Basin. The second rock type evaluated is a proxy for sediments from the United States Gulf Coast. The third rock type is a dunite, an essentially monomineralic rock consisting of olivine. Xu et al. (2004b)

presented simulation results on mass transfer, mineral alteration, and consequent CO_2 sequestration in a sandstone-shale system.

Here we present a numerical simulation for the injection of CO_2, H_2S and SO_2 mixtures in a sandstone-shale sequence using hydrogeologic properties and mineral compositions commonly encountered in Gulf Coast sediments. Simulations were performed with the reactive fluid flow and geochemical transport code TOUGHREACT (Xu and Pruess, 2001; Xu et al., 2004c). 1-D and 2-D regions around a injection well were considered for sandstone alone and a sandstone-shale sequence, respectively, to analyze mineral alteration, acid-gas immobilization through precipitation, and changes in porosity.

2. Numerical Modeling Approach

2.1. Simulation method

The present simulations were carried out using the non-isothermal reactive geochemical transport code TOUGHREACT (Xu and Pruess, 2001; Xu et al., 2004c). This code was developed by introducing reactive chemistry into the framework of the existing multi-phase fluid and heat flow code TOUGH2 (Pruess et al., 1999). Our modeling of flow and transport in geologic media is based on space discretization by means of integral finite differences (Narasimhan and Witherspoon, 1976). An implicit time-weighting scheme is used for the individual components of the model consisting of flow, transport, and kinetic geochemical reactions. TOUGHREACT uses a sequential iteration approach similar to that described by Yeh and Tripathi (1991). After solution of the flow equations, the fluid velocities and phase saturations are used for chemical transport simulation. The chemical transport is solved on a component basis. The resulting concentrations obtained from the transport are substituted into the chemical reaction model. The system of chemical reaction equations is solved on a grid-block basis by Newton-Raphson iteration, similar to Parkhurst et al. (1980), Reed (1982), and Wolery (1992). The chemical transport and reaction equations are iteratively solved until convergence. Full details on the numerical methods are given in Xu and Pruess (2001) and Xu et al. (2004c).

2.2. Process capabilities

The TOUGHREACT simulator can be applied to one-, two-, or three-dimensional porous and fractured media with physical and chemical heterogeneity, and can accommodate any number of chemical species present in liquid, gas and solid phases. A wide range of subsurface thermo-physical-chemical processes is considered. The major processes considered for fluid and heat flow are: (1) fluid flow in both liquid and gas phases under pressure and gravity forces, (2) capillary pressure effects for the liquid phase, and (3) heat flow by conduction, convection and diffusion. The transport of

aqueous and gaseous species by advection and molecular diffusion is considered in both liquid and gas phases.

Aqueous chemical complexation and gas (CO_2) dissolution and exsolution are assumed to be locally at equilibrium. Because most homogeneous reactions in the aqueous phase are almost instantaneous, they can be effectively considered at equilibrium. Coupled redox reactions are formulated in terms of dissolved oxygen, where the chemical potential of the dissolved oxygen can be related to the oxidation state of the system (Nordstrom and Muñoz, 1986; Wolery, 1992). In natural systems, some redox reactions (such as sulfite/sulfide) that take place homogeneously within the aqueous phase are slow to achieve equilibrium, and therefore violate the local equilibrium assumption inherent in the current formulation of TOUGHREACT. This is consistent with observed discrepancies between the potentials estimated from different redox pairs (Stumm and Morgan, 1981). However, the validity of the local equilibrium assumption depends on the rate of transport relative to the rate of reaction. For long simulation times (such as 10,000 years in present simulations), a chemical equilibrium assumption is justified under certain circumstances. Mineral dissolution and precipitation can be modeled subject to either local equilibrium or kinetic conditions. The kinetic rate law used is given in Section 2.4.

The activity of aqueous species is equal to the product of the activity coefficient and molar concentration (mol/kg H_2O). Aqueous species activity coefficients with the exception of CO_2(aq) are calculated from the extended Debye-Hückel equation (Helgeson et al., 1981). CO_2(aq) activity coefficient and CO_2(g) fugacity coefficient are functions of pressure, temperature and salinity (details on calculations are given in Xu et al., 2004a).

Changes in porosity and permeability due to mineral dissolution and precipitation can modify fluid flow. This interaction between flow and chemistry can be important and is considered in our model. Changes in porosity during the simulation are calculated from changes in mineral volume fractions. Several models were considered to calculate changes in permeability due to changes in porosity (Xu et al., 2004c).

2.3. Thermodynamic data

The quality and accuracy of geochemical modeling is enhanced through the use of internally consistent and critically evaluated thermodynamic data derived from a comprehensive review of the published literature. The primary source for equilibrium constants for aqueous species and minerals used in this study originated with the EQ3/6 V7.2b database (Wolery, 1992). However, many substitutions and changes have been incorporated in response to more recent published revisions in the thermodynamic properties of several rock-forming minerals and aqueous species. Among these are revisions to the properties of feldspar by Arnorsson et al. (1999), several clay minerals by Kulik and Aja (1997), and dawsonite (Ferrante et al., 1976). In addition, a comprehensive revision to the properties of silica polymorphs and SiO_2(aq) was initiated in response to refined low temperature quartz solubility measurements. Revised thermodynamic properties of relevant aqueous species based on the Helgeson-Kirkham-Flowers (HKF) equation of state (Shock et al., 1997), including aluminum species were also incorporated. Changes in the properties of SiO_2(aq) and AlO_2^- necessitated recomputation of the solubility products for all minerals containing silica or alumina components, whose thermodynamic properties were based on calorimetric measurements.

To ensure consistency with unmodified equilibrium constants in the EQ3/6 V7.2b database, previously generated from thermodynamic data using SUPCRT92 (Johnson et al., 1992), all revised thermodynamic data were incorporated in the SUPCRT92 database and new equilibrium constants were similarly generated.

In addition to the changes noted above, the thermodynamic properties of several other phases, including carbonates, chlorite, kerogen-OS, and the ferrous and ferric ion related minerals, were estimated and their solubility products incorporated to improve model verisimilitude. Details are given in Xu et al. (2004b).

2.4. Kinetic data

For kinetically-controlled mineral dissolution and precipitation, a general form of rate law (Lasaga, 1984; and Steefel and Lasaga, 1994) is used

$$r_m = \pm k_m A_m a_{H^+}^n \left| \left[\left(\frac{Q_m}{K_m} \right)^{\mu} - 1 \right] \right|^{\nu} \tag{1}$$

where m is mineral index, r_m is the dissolution/precipitation rate (positive values indicate dissolution, and negative values precipitation), A_m is the specific reactive surface area per kg H_2O, k_m is the temperature-dependent rate constant (moles per unit mineral surface area and unit time), a_{H^+} is the activity of H^+ and n is empirical reaction order accounting for catalysis by H^+ in solution. K_m is the equilibrium constant for the mineral-water reaction written for the destruction of one mole of mineral m, Q_m is the reaction quotient, the parameters μ and ν are positive numbers normally determined by experiment, and are usually, but not always, taken as equal to unity (as in the present work). The temperature dependence of the reaction rate constant can be expressed reasonably well via an Arrhenius equation (Lasaga, 1984; and Steefel and Lasaga, 1994). Since many rate constants are reported at 25 ^{o}C (298.15 K), it is convenient to approximate the functional dependency of the rate constant on temperature, thus

$$k = k_{25} \exp\left[\frac{-E_a}{R} \left(\frac{1}{T} - \frac{1}{298.15} \right) \right] \tag{2}$$

where E_a is the activation energy, k_{25} is the rate constant at 25 ^{o}C, R is the gas constant, and T is absolute temperature.

Mineral dissolution and precipitation rates are a product of the kinetic rate constant and reactive surface area (Eq. 1). The parameters used for the kinetic rate expression are given in Table 1. Calcite is assumed to react at equilibrium because its reaction rate is typically quite rapid relative to the time frame being modeled. In Table 1,

we include separate rate constants (k_{25}), activation energies (E_a), and the reaction order (n) for each mechanism (acid catalyzed and no catalysis). At any pH the total rate is the sum of the rates from all mechanisms. The acid catalysis is considered only for mineral dissolution. Some kinetic parameters were taken directly from the published scientific literature. The references are listed in the fifth column of Table 1. Others were assigned with values from similar minerals with known kinetic properties. The evolution of surface area in natural geologic media is very complex, especially for multi-mineralic systems, and is not quantitatively understood at present. Mineral reactive surface areas (last column of Table 1) were taken from Sonnenthal and Spycher (2001), which were calculated assuming a cubic array of truncated spheres constituting the rock framework. For the clay minerals kaolinite, illite, and smectite, surface areas were increased to account for reactive edges in these sheet silicate minerals (Nagy, 1995). The kinetic rate constants given in Table 1 were normalized to BET surface areas in the original studies. The geometric surface areas should be normalized to BET surface areas according to the roughness factor of individual minerals. A reactive surface area calculated from grain size may give a poor estimate of the hydrologically accessible mineral surface area. Furthermore, in multi-mineralic field scale systems the reactive surface area for a given mineral is generally smaller due to many factors such as coating. To account for these effects, surface areas listed in Table 1 were arbitrarily reduced by one order of magnitude in the present simulations.

The precipitation of possible secondary minerals is represented using the same kinetic expression as for dissolution. However, several aspects regarding precipitation are different from dissolution, including nucleation, crystal growth and Ostwald ripening processes, as well as the calculation of the reactive surface area (Steefel and van Capellen, 1990). These processes affecting mineral precipitation are not considered in the current model.

Table 1. List of kinetic rate parameters used in Eqs. (1) and (2) for minerals considered in the present simulations (The rate constant k_{25} is for far from equilibrium conditions).

Mineral	k_{25} (moles $m^{-2}s^{-1}$)	E_a (KJ/mol)	n	Reference	Surface area (cm^2/g)
anhydrite	Equilibrium				
calcite	Equilibrium				
quartz	$1.26x10^{-14}$	87.50	0	Tester et al. (1994)	9.8
K-feldspar	$1.00x10^{-12}$	57.78	0	Blum and Stillings (1995)	9.8
	$3.55x10^{-10}$	51.83	0.4	Blum and Stillings (1995)	9.8
kaolinite	$1.00x10^{-13}$	62.76	0	Nagy (1995)	151.6
	$4.37x10^{-12}$	62.76	0.17	Nagy (1995)	151.6
magnesite	$4.47x10^{-10}$	62.76	0	Chou et al. (1989)	9.8
	$4.37x10^{-5}$	18.98	1.0	Chou et al. (1989)	9.8
siderite	$1.26x10^{-9}$	62.76	0	Steefel (2001)	9.8
	$1.02x10^{-3}$	20.90	0.9	Gautelier et al. (1999)	9.8
dolomite	$1.26x10^{-9}$	62.76	0	Set to siderite	9.8
	$1.02x10^{-3}$	20.90	0.9	Set to siderite	9.8
ankerite	$1.26x10^{-9}$	62.76	0	Set to siderite	9.8
	$1.02x10^{-3}$	20.90	0.9	Set to siderite	9.8
dawsonite	$1.26x10^{-9}$	62.76	0	Set to siderite	9.8
	$1.02x10^{-3}$	20.90	0.9	Set to siderite	9.8
kerogen-OS	$1.00x10^{-13}$	0.0	0.0	Assumed	10
oligoclase	$1.00x10^{-12}$	57.78	0	Set to K-feldspar	10
	$3.55x10^{-10}$	51.83	0.4	Set to K-feldspar	10
albite-low	$1.00x10^{-12}$	67.83	0	Blum and Stillings (1995)	9.8
	$2.04x10^{-10}$	59.77	0.5	Blum and Stillings (1995)	9.8
Na-smectite	$1.00x10^{-13}$	62.76	0	Set to kaolinite	151.6
	$4.37x10^{-12}$	62.76	0.17	Set to kaolinite	151.6
Ca-smectite	$1.00x10^{-13}$	62.76	0	Set to kaolinite	151.6
	$4.37x10^{-12}$	62.76	0.17	Set to kaolinite	151.6
illite	$1.00x10^{-13}$	62.76	0	Set to kaolinite	151.6
	$4.37x10^{-12}$	62.76	0.17	Set to kaolinite	151.6
pyrite	$4.00x10^{-11}$	62.76	0	Ague and Brimhall (1989)	12.9
hematite	$4.00x10^{-11}$	62.76	0	Set to pyrite	12.9
chlorite	$2.51x10^{-12}$	62.76	0	Malmstrom et al. (1996)	9.8
alunite	$1.00x10^{-12}$	57.78	0	Set to K-feldspar	9.8

3. Problem Setup

3.1. Fluid flow conditions

Much specific and detailed information is required to assess the feasibility of injection of CO_2 - H_2S or SO_2 mixtures in a sandstone-shale formation at any particular site, and to develop engineering designs for acid-gas injection systems. Before conducting site-specific investigations, general features and issues relating to the injected formation should be explored. This can be done by investigating a sandstone-shale system, which abstracts site-specific features, and thereby attempts to represent characteristics that are common to many such systems. A basic issue is the geochemical behavior of acid-gas mineral trapping in a sandstone-shale system under high gas pressure injection conditions.

Only one layer of sandstone and one layer of shale are considered in the present model (Figure 1). Hydrological parameter specifications for sandstone and shale layers were chosen to be representative of conditions that may be encountered in Texas Gulf Coast sediments at a depth of order 2 km (Table 2). Two fluid flow systems are considered. The first considers only the sandstone layer, neglecting fluid flow and chemical transport in the shale layer. The second considers both layers to illustrate effects of shale on acid-gas sequestration and mass transfer between the two layers. The geologic formation is assumed to extend infinitely in horizontal dimensions. Radial grids are used for the horizontal direction with spacing increasing away from the well. For the sandstone-shale system, due to the symmetric configuration, only half of the sandstone (5 m) and half of the shale (5 m) layer thickness were modeled. A total of 9 vertical grid blocks were used for the shale layer with finer spacing near the interface between the sandstone and the shale to better resolve concentration gradients in the low permeability shale. Only one grid block in the vertical direction was used for the sandstone layer and the calculation point for this block was placed at the interface with the shale, representing a conceptual model of perfect mixing throughout the sand.

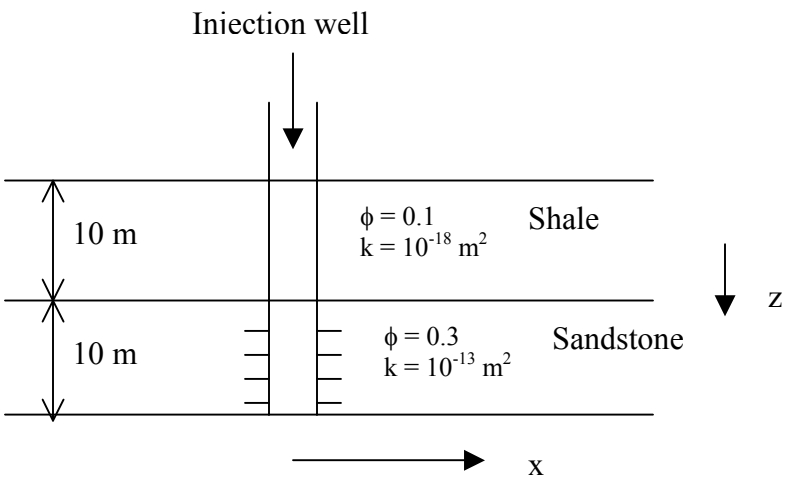

Figure 1. Simplified radial flow model for a sandstone-shale system.

The fluid property module ECO2 used in TOUGHREACT considers only three components of supercritical CO_2, water, and brine. Co-injection of H_2S and SO_2 is achieved by dissolving these gases in water. The injection rates of CO_2, water, H_2S and SO_2 for four different cases are given in Table 3. The first case injects only CO_2 and water (base case). The other three cases inject H_2S or SO_2 or H_2S+SO_2 with 99 wt% of CO_2. Fluid injection was applied only to the sandstone portion (Figure 1).

Table 2. Hydrogeologic parameters for sandstone and shale layers.

Parameters	Sandstone	Shale
Permeability (m^2) Porosity Tortuosity Compressibility (Pa^{-1}) Diffusivity (m^2/s)	10^{-13} 0.3 0.3 $1x10^{-8}$ $1x10^{-9}$	10^{-18} 0.1 0.1 $1x10^{-8}$ $1x10^{-9}$
Relative permeability		
Liquid (van Genuchten, 1980): $k_{rl} = \sqrt{S^*}\left\{1-\left(1-\left[S^*\right]^{1/m}\right)^m\right\}^2$ S_{lr} : irreducible water saturation m: exponent	$S^* = (S_l - S_{lr})/(1-S_{lr})$ $S_{lr} = 0.00$ $m = 0.457$	$S_{lr} = 0.00$ $m = 0.457$
Gas (Corey, 1954):		
$k_{rg} = (1-\widehat{S})^2(1-\widehat{S}^2)$ S_{gr} : irreducible gas saturation	$\widehat{S} = \frac{(S_l - S_{lr})}{(S_l - S_{lr} - S_{gr})}$ $S_{gr} = 0.05$	$S_{gr} = 0.05$
Capillary pressure		
van Genuchten (1980) $P_{cap} = -P_0\left(\left[S^*\right]^{-1/m} - 1\right)^{1-m}$ S_{lr} : irreducible water saturation m: exponent P_0 : strength coefficient	$S^* = (S_l - S_{lr})/(1-S_{lr})$ $S_{lr} = 0.00$ $m = 0.457$ $P_0 = 19.61\,kPa$	$S_{lr} = 0.00$ $m = 0.457$ $P_0 = 6.2\,MPa$

Table 3. Injection rates (kg/s, over 5 m thickness sandstone layer) of different chemical components.

Case	*CO_2*	*Water*	*H_2S*	*SO_2*
CO_2 only	0.5	0.25		
CO_2 with H_2S	0.5	0.245	0.005	
CO_2 with SO_2	0.5	0.245		0.005
CO_2 with H_2S and SO_2	0.5	0.245	0.0025	0.0025

For the sandstone alone or the sandstone-shale sequence, four reactive geochemical transport simulations corresponding to the combination of injection of different acid gases (Table 3) were performed. Injection was assumed to continue for a period of 100 years. The fluid flow and geochemical transport simulations were run for a period of 10,000 years.

The present simulation does not consider non-uniform sweep that may occur due to formation heterogeneities, or to buoyancy forces that would tend to drive gases towards the top of the sandstone. In future studies we plan to examine such multidimensional flow effects. Some justification for these omissions can be made by considering the slow rates and long time scales of geochemical processes, which will make the distribution of gases to be more uniform. Initially, injected gases will tend to accumulate and spread out near the top of permeable intervals, partially dissolving in the aqueous phase. Gas dissolution causes the aqueous-phase density to increase by a few percent. This will give rise to buoyant convection where waters enriched in gas will tend to migrate downward (Weir et al., 1995; Garcia, 2001; Ennis-King and Paterson, 2003). The process of gas dissolution and subsequent aqueous phase convection will tend to mix aqueous species in the vertical direction. The time scale for significant convective mixing is likely to be slow, on the order of hundreds of years (Ennis-King and Paterson, 2003), and may be roughly comparable to time scales for significant geochemical interactions of the acid gases with minerals comprising the rock matrix.

3.2. Geochemical conditions

A proxy for sandstone-shale sequences from the United States Gulf Coast was used as a basis for the geochemical simulation. Although our simulation addresses a particular case, the results have a broader application to other sedimentary basins. The initial mineral composition of sandstone and shale layers used in the present modeling (Table 4), was taken from a previous batch geochemical modeling study (Xu et al., 2004a). The specification of formation mineralogy is determined in part by the availability of data. Most studies related to Tertiary Gulf Coast sediments are concentrated in the state of Texas. The principal reservoir-quality sandstones within that region are respectively, the Frio, the Vicksberg and the Wilcox formations, all of which are found within the Lower Tertiary. Of the three formations, the Frio was chosen as a representative candidate for the sequestration of acid gases. The model shale composition is based on the recent study by Land et al. (1997) of Upper Oligocene - Lower Miocene mudrocks. Details on the selection of mineral composition are given in Xu et al. (2003b). Because H_2S and SO_2 are injected in addition to CO_2 in the current modeling, anhydrite and alunite were included as possible secondary phases.

Not all primary and possible secondary phases listed in Table 4 were present in the system at a given time. For example, dolomite and Ca-smectite were included in the list of possible secondary mineral phases for the simulations, but they did not form. The system had not attained equilibrium after the simulation time period, but had settled down to a quasi steady-state condition. Therefore, the number of phases present at any time differs in number for that predicted by the phase rule under equilibrium conditions. It is understood that detrital mineral assemblages do not normally obey Gibb's Phase Rule, as they also are not at equilibrium.

Table 4. List of initial mineral volume fractions and possible secondary mineral phases for sandstone and shale layers.

Mineral	Chemical composition	Vol.% of solid rock		Vol.% of medium	
		Sandstone	Shale	Sandstone	Shale
***Primary*:**					
quartz	SiO_2	58	19.22	40.6	17.3
kaolinite	$Al_2Si_2O_5(OH)_4$	2.02	4.37	1.41	3.95
calcite	$CaCO_3$	1.93	10.9	1.35	9.81
illite	$K_{0.6}Mg_{0.25}Al_{1.8}(Al_{0.5}Si_{3.5}O_{10})(OH)_2$	1.0	28.14	0.7	25.33
kerogen-OS	$C_{64}H_{102}O_{40}S_{10}$	0.0	2.0	0.0	1.8
oligoclase	$CaNa_4Al_6Si_{14}O_{40}$	19.8	5.28	13.86	4.75
K-feldspar	$KAlSi_3O_8$	8.2	4.74	5.74	4.27
Na-smectite	$Na_{0.290}Mg_{0.26}Al_{1.77}Si_{3.97}O_{10}(OH)_2$	4	23.0	2.8	20.7
chlorite	$Mg_{2.5}\ Fe_{2.5}Al_2Si_3O_{10}(OH)_8$	4.55	2.35	3.19	2.12
hematite	Fe_2O_3	0.5	0.0	0.35	0.0
porosity	----	----	----	30	10
***Secondary*:**					
anhydrite	$CaSO_4$				
magnesite	$MgCO_3$				
low-albite	$NaAlSi_3O_8$				
dolomite	$CaMg(CO_3)_2$				
siderite	$FeCO_3$				
Ca-smectite	$Ca_{0.145}Mg_{0.26}Al_{1.77}Si_{3.97}O_{10}(OH)$				
pyrite	FeS_2				
ankerite	$CaMg_{0.3}Fe_{0.7}(CO_3)_2$				
dawsonite	$NaAlCO_3\ (OH)_2$				
alunite	$KAl_3\ (OH)_6(SO_4)_2$				

Prior to simulating reactive transport in the sandstone-shale system, batch geochemical modeling of water-rock interaction was performed for sandstone and shale sepqrately, to obtain a nearly equilibrated water chemistry. A pure 1.0 M solution of sodium chloride and CO_2 gas pressure of 1×10^{-2} bar were used reacting with the primary minerals listed in Table 4 at a temperature of 75°C, that is based on a land surface temperature of 15°C and a geothermal gradient of 30°C/km. A reasonable short time of simulation (10 years in the present study) is needed to obtain a quazi-steady state when changes in aqueous concentrations and changes in mineral abundances are very slightly. The resulting water chemistry (Table 5) was used for the initial condition of reactive geochemical transport simulations.

Gulf Coast Formation waters were not used to specify the initial groundwater composition in the simulation, because a choice of formation water would not represent an initial equilibrium state with respect to the secondary mineralogy in our simulations. Thus, we chose to generate our own initial aqueous phase composition through *a priori* simulation of the ambient state. It should be noted that Gulf Coast formation waters vary substantially in composition for many reasons. Our simulated initial composition given in Table 5 generally falls within the range of compositions for Gulf Coast formation waters where total $Cl^- \approx 1.0$ mol/kg H_2O, e.g. see Kreitler and Richter (1986). Because we focused our attention on high-pressure CO_2 simulations, the initial water composition affects geochemical evolution for only a short time period after initialization.

Table 5. Initial total dissolved component concentrations (mol/kg H_2O) for reactive transport simulations in the sandstone-shale system. (Iron is the sum of Fe^{+2} , Fe^{+3} and their related complexes. Carbon is the sum of CO_2(aq), CH_4(aq), and their related species such as HCO_3^- and acetic acid(aq). Sulfur is the sum of sulfate and sulfide species)

Component	Sandstone	Shale
Ca^{+2}	3.23×10^{-3}	6.463×10^{-2}
Mg^{+2}	4.531×10^{-8}	3.121×10^{-7}
Na^+	1.037	1.071
K^+	5.672×10^{-5}	2.515×10^{-4}
Iron	1.118×10^{-5}	1.235×10^{-3}
SiO_2(aq)	1.939×10^{-3}	1.919×10^{-3}
Carbon	4.463×10^{-2}	4.173×10^{-2}
Sulfur	1.00×10^{-9}	1.205×10^{-7}
Al^{+3}	7.87×10^{-8}	8.334×10^{-9}
Cl^-	1.0	1.0
pH	7.34	6.69
Temperature	75°C	75°C

4. Results and Discussion

4.1. Sandstone alone

The fluid flow pattern obtained with different injection rates of acid gases as listed in Table 3 is very similar. Figure 1 shows water saturations along the radial distance (gas CO_2 saturations are complementary to water saturations, or $S_g = 1- S_l$). The reactive geochemical transport modeling results obtained from the CO_2 only case are similar to those from CO_2 with H_2S. The results from CO_2 with SO_2 case are similar to those from CO_2 with SO_2 and H_2S. Therefore, the results of CO_2 only and CO_2 with SO_2 injection cases will be presented here.

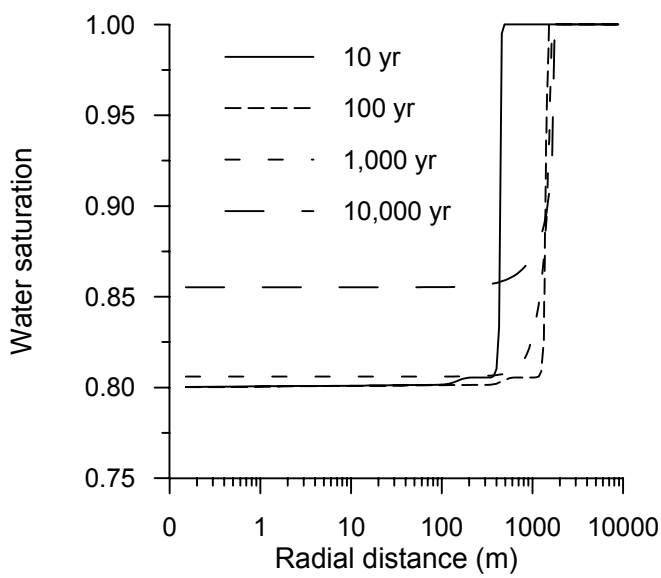

Figure 1. Water saturations along radial distance at different times.

The pH distribution along the radial distance is presented in Figure 2. For the CO_2 only case, pH is the lowest (3.4) close to the well after 10 years. This can be explained by the temporal profile of pH evolution and calcite dissolution at 1.25 m, which is presented in Figure A.1 in Appendix A. The injected CO_2 causes the pH to trend lower, but calcite dissolution consumes H^+ and increases pH. Calcite dissolution is very fast in relative to the duration of the simulation and is assumed at equilibrium. After about 0.4 years calcite disappears and pH dramatically decreases to a minimum value of 3.4. The minimum pH

remains until about 10 years when some minerals such as kaolinite start to precipitate. The initial precipitation depends on precipitation kinetics of the secondary minerals. After 10 years, pH is buffered by CO_2 injection and mineral alteration. After 100 years when the injection ceases, the effects of mineral alteration cause pH to increase, until 1000 years, a pH of about 6 is attained.

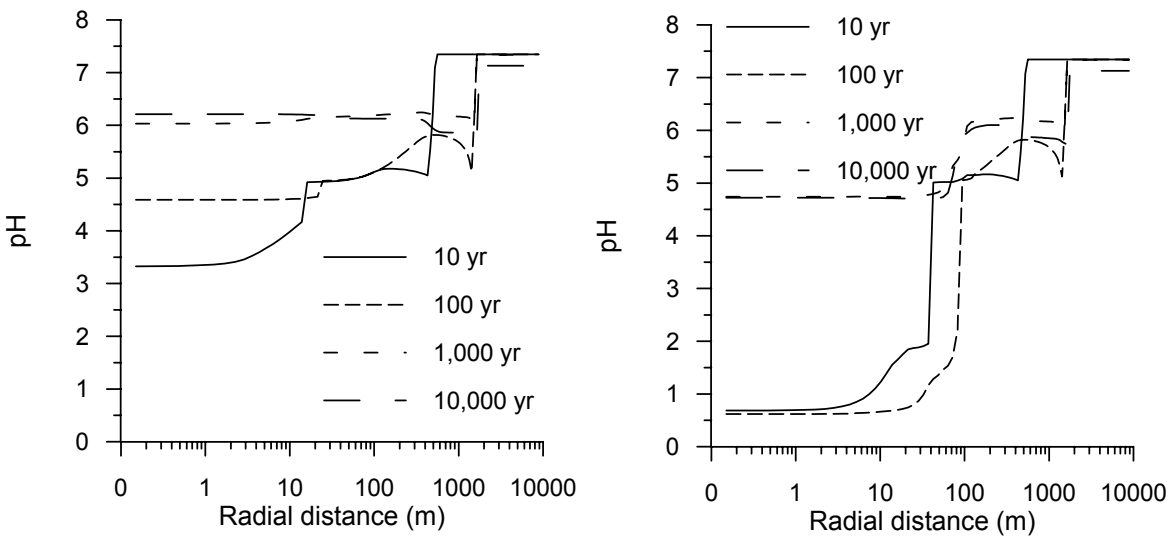

Figure 2. pH distribution at different times for sandstone alone.

A much lower pH (about 0.6) resulted from injection of CO_2 with SO_2 (Figure 2b). After 100 yr, this extremely acidified zone extends to a radial distance of close to 100 m. SO_2 has a very strong effect on lowering pH because of the disproportionation reaction:

$$4SO_2 + 4H_2O \rightarrow 3HSO_4^- + H_2S + 3H^+$$

Sulfuric acid generation has been observed in magmatic hydrothermal systems and confirmed by lab experiments (Kusakabe et al., 2000). In this SO_2 injection case, calcite disappears much sooner (after 0.01 years, see also Figure A.3 in Appendix A). The low pH of 0.6 is maintained until 100 years when injection of CO_2 with SO_2 ceases. Corrosion and well abandonment would be an important issue with SO_2 injection.

Dissolution and precipitation of minerals occurring in both CO_2 only and CO_2 with SO_2 cases are presented in Figures 3 through 14. To facilitate comparison, results obtained from CO_2 only are placed on the left side of each figure, while those from CO_2 with SO_2 are placed on the right side. Calcite dissolution close to the well bore is quite rapid in both cases (Figure 3). More K-feldspar dissolves within a 100 m distance with CO_2 plus SO_2 mixture than with CO_2 only due to the lower pH (Figure 4). The pattern of oligoclase dissolution is similar to that of K-feldspar (Figure 5). Chlorite dissolution occurs in all cases (Figure 6). Slight dissolution of hematite also occurs.

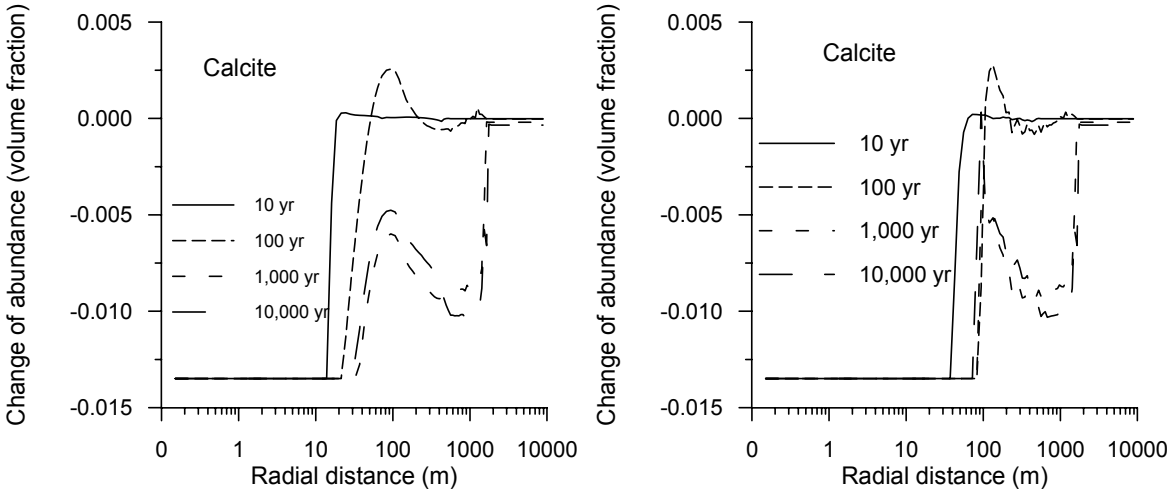

(a) CO_2 (b) CO_2+ SO_2

Figure 3. Change of calcite abundance in the sandstone at different times (negative values indicate dissolution and positive precipitation)

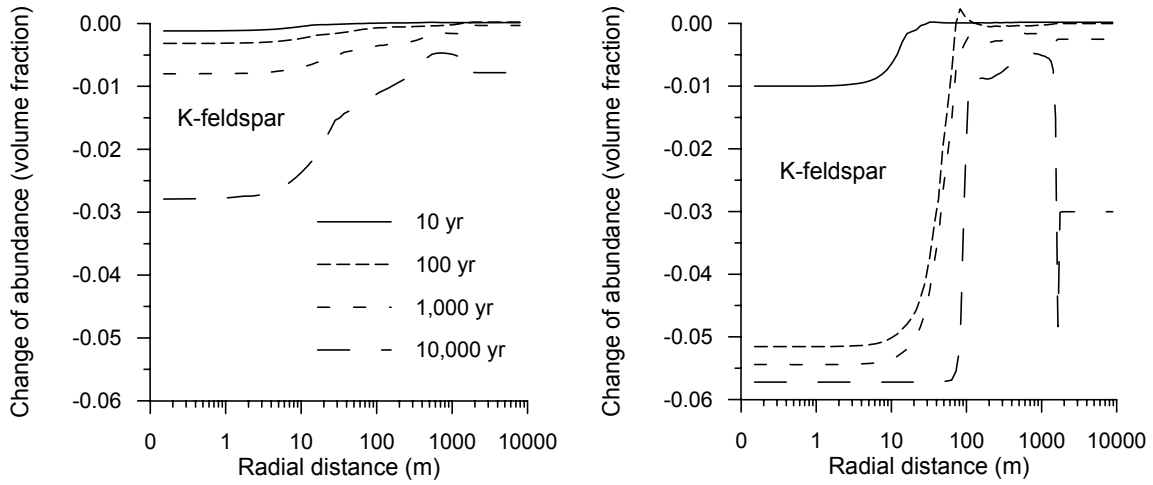

(a) CO_2 (b) CO_2+ SO_2

Figure 4. Change of K-feldspar abundance at different times

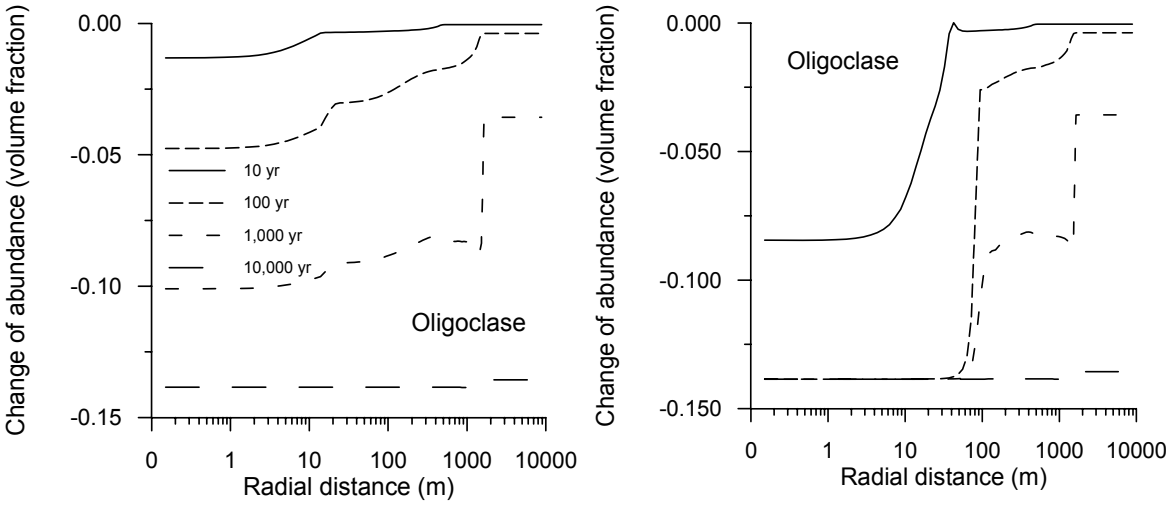

(a) CO_2 (b) CO_2+ SO_2

Figure 5. Change of oligoclase abundance at different times

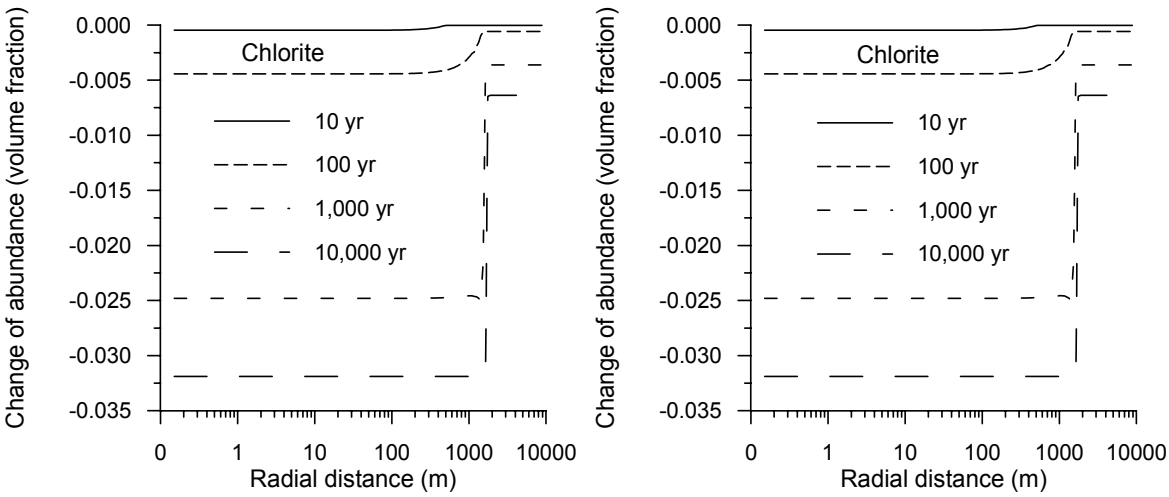

(a) CO_2 (b) CO_2+ SO_2

Figure 6. Change of chlorite abundance at different times.

As primary minerals dissolve, secondary phases are formed. Precipitation of quartz is extensive in both cases (Figure 7). For the CO_2 only case, significant precipitation of illite and kaolinite occurs in the distance range from 0 to 10 m (Figures 8 and 9). For the CO_2 with SO_2 case, very slight precipitation of these two minerals occurs in the 0 - 10 m range because of the extremely low pH (0.6), but precipitation is at a maximum at a distance of about 50 m. Peaks of maximum quartz precipitation also occur when SO_2 is injected with CO_2. For the CO_2 injection only, precipitation of Na-smectite is extensive within the entire plume of injected CO_2 (Figure 10), but for CO_2 + SO_2 injection the precipitation of Na-smectite is not significant within the 0-50 m range.

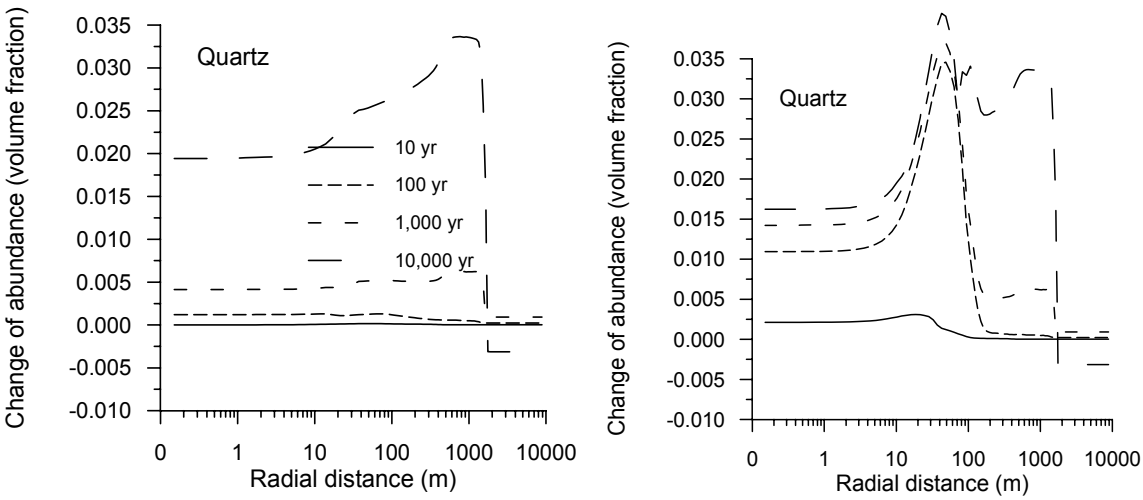

(a) CO_2 (b) CO_2+ SO_2

Figure 7. Change of quartz abundance at different times

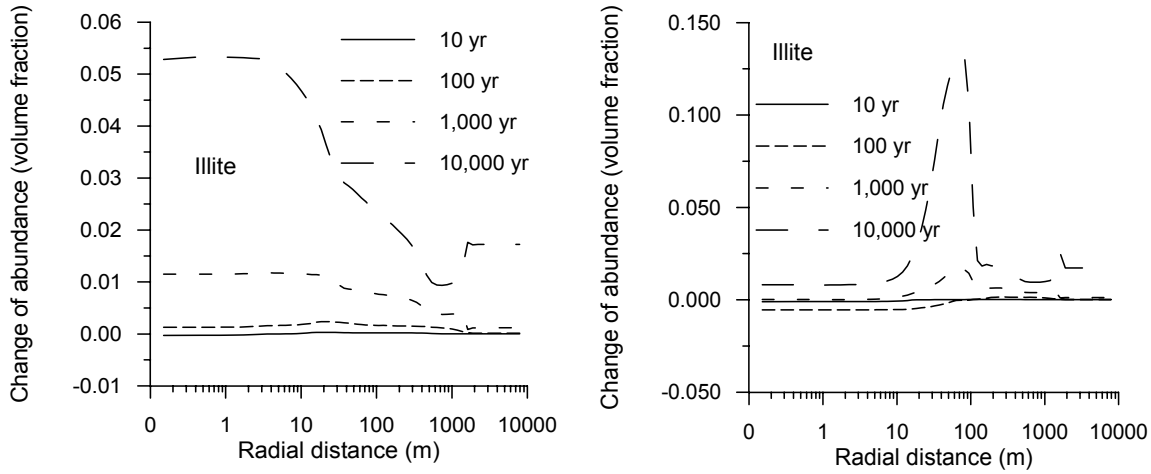

(a) CO_2 (b) CO_2+ SO_2

Figure 8. Change of illite abundance at different times

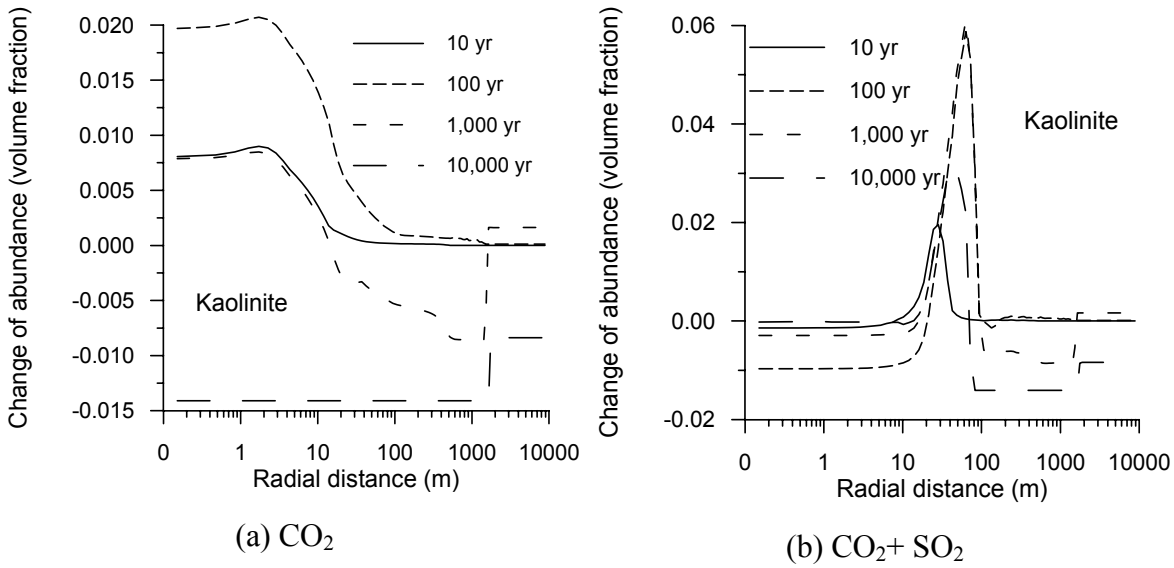

(a) CO_2 (b) CO_2+ SO_2

Figure 9. Change of kaolinite abundance at different times

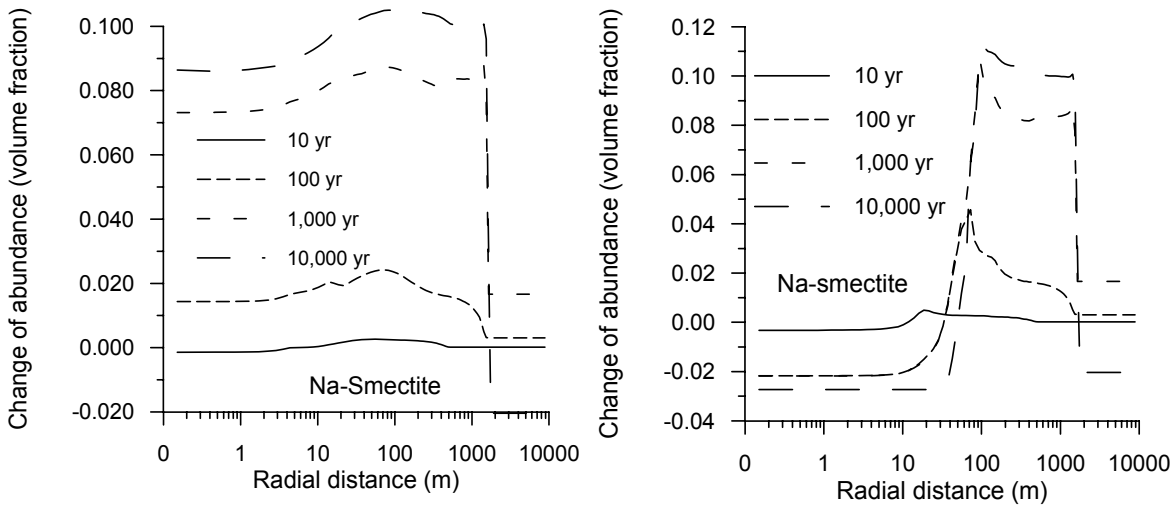

(a) CO_2 (b) CO_2+ SO_2

Figure 10. Change of Na-smectite abundance at different times

The injected CO_2 is immobilized by precipitation of four carbonate minerals: magnesite ($MgCO_3$), siderite ($FeCO_3$), ankerite ($CaMg_{0.3}Fe_{0.7}(CO_3)_2$), and dawsonite ($NaAlCO_3(OH)_2$). A minor amount of magnesite precipitates in the acidified zones close to the wellbore (Figure 11). Some of the CO_2 is trapped by precipitation of siderite (Figure 12). For injection of CO_2 with SO_2, after 10,000 years a total of 1.2% of volume

fraction of siderite precipitates in acidified zone (in the 100 m radial distance range). Significant CO_2 is immobilized by precipitation of ankerite (Figure 13). After 10,000 years a maximum of 4% of volume fraction of ankerite is formed at about 1000 m from the injection well. For co-injection of SO_2, no ankerite precipitation occurs in the acidified zone. Significant dawsonite also precipitates, its pattern is similar to ankerite (Figure 14). No dolomite ($CaMg(CO_3)_2$) precipitation is observed in the simulations. Calcite dissolves under the acid-gas injection conditions (Figure 3).

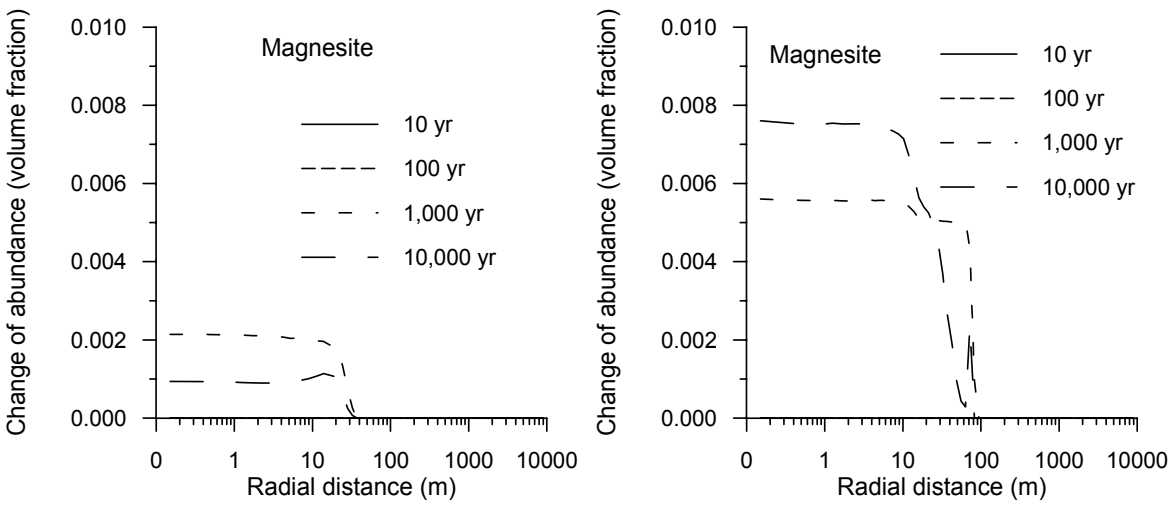

(a) CO_2 (b) CO_2+ SO_2

Figure 11. Change of magnesite abundance at different times.

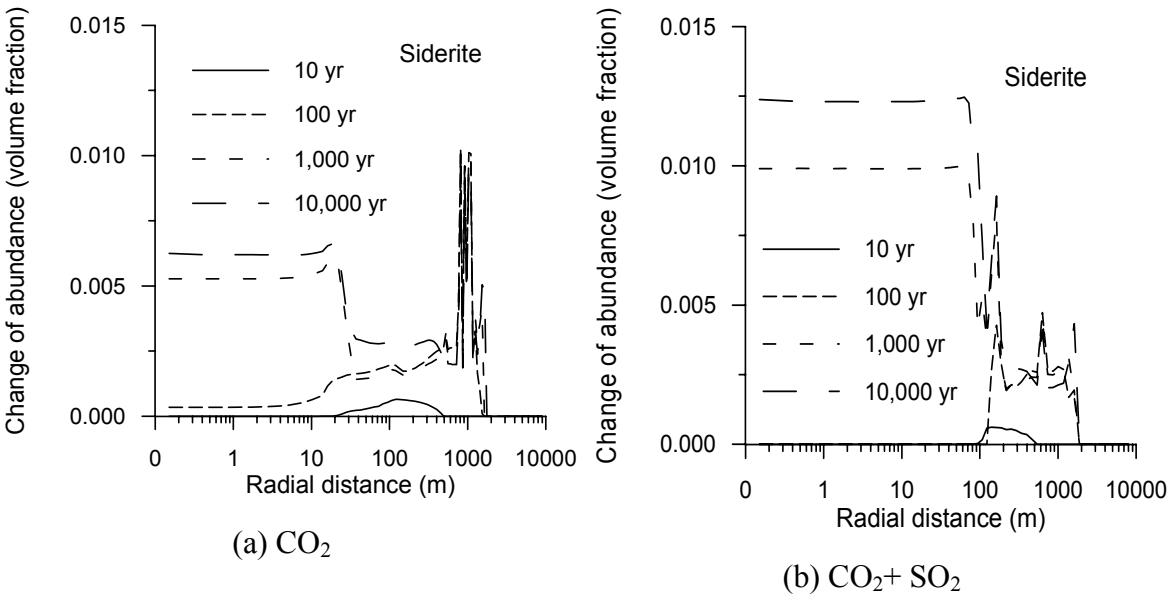

Figure 12. Change of siderite abundance at different times

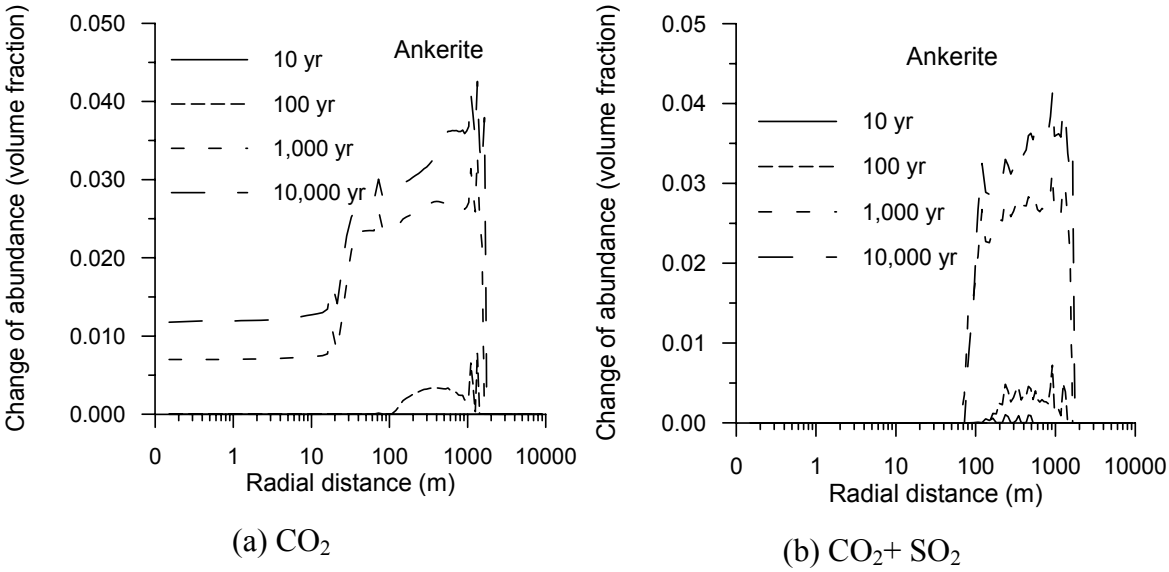

Figure 13. Change of ankerite abundance at different times.

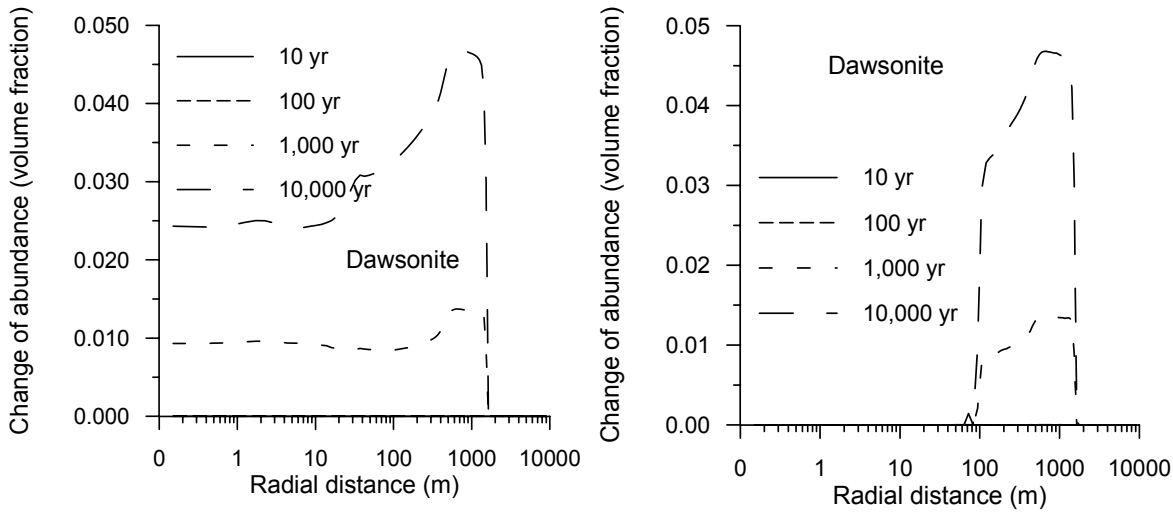

(a) CO_2 (b) CO_2+ SO_2

Figure 14. Change of dawsonite abundance at different times

The total amount of CO_2 sequestered in minerals, mainly as ankerite and dawsonite, but with some siderite, is presented in Figure 15. As expected, no CO_2 is sequestered in mineral phases in the acidified zone during the injection operation period of 100 years, but calcite dissolves. Injecting CO_2 creates an acidified zone only within a 20 m radius. Injecting CO_2 with SO_2 creates a much larger and stronger acidified zone with a radius of 100 m. After 100 years, minor amounts of CO_2 are sequestered by carbonate precipitation in these acidified zones. Most CO_2 mineral sequestration occurs beyond the acidified zones. After 10,000 years, the CO_2 mineral trapping capability can reach 76 kg per cubic meter of medium. Temporal profiles of pH, mineral abundance and porosity at 1000 m radial distance (within the CO_2 mineral trapping zone) are given for the CO_2 injection only case in Figure A.2 in Appendix A. We here show the cumulative CO_2 sequestration profile in Figure 16, using a linear scale (instead of log10 scale, as in Figure A.2). From this figure, we can see that after 10,000 years, CO_2 sequestration by carbonate precipitation is very close to the expected maximum. The CO_2 trapping capability depends on the primary mineral composition. Precipitation of siderite and ankerite requires Fe^{2+} supplied by chlorite ($Mg_{2.5}Fe_{2.5}Al_2Si_3O_{10}(OH)_8$) dissolution. Precipitation of dawsonite requires Na^+ provided by oligoclase ($CaNa_4Al_6Si_{14}O_{40}$) dissolution. The initial abundance of chlorite and oligoclase therefore affects the CO_2

mineral trapping capability. The sequestration time required depends on the kinetics of mineral dissolution and precipitation.

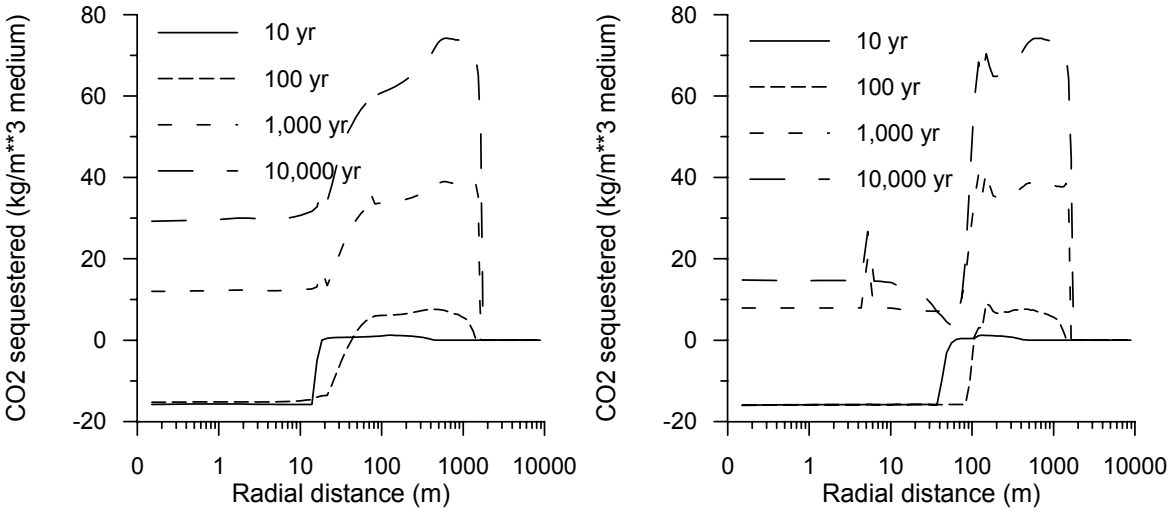

(a) CO_2 (b) CO_2+ SO_2

Figure 15. Cumulative CO_2 sequestered by carbonate mineral precipitation at different times.

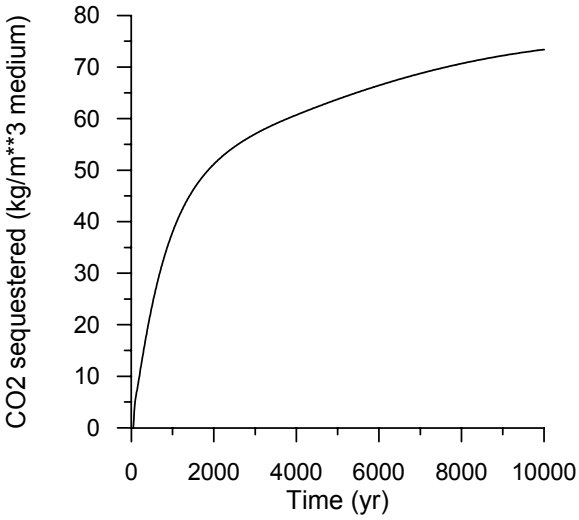

Figure 16. Cumulative CO_2 sequestration with time at 1000 m distance (injection of CO_2 only case).

Now we report simulated changes in mineral abundances due to disproportionation of SO_2. Precipitation of sulfur bearing minerals pyrite (FeS_2), anhydrite ($CaSO_4$), and alunite ($KAl_3(OH)_6(SO_4)_2$) occurs (Figure 17). Pyrite precipitates in the acidified zone up to a radial distance of about 100 m, with a minor amount of 0.45% volume fraction. Pyrite also forms in the CO_2 with H_2S case. Anhydrite precipitation initially occurs in the 0 – 100 m range, but is later confined to a distance between 10 – 100 m, with a maximum volume fraction of 2.7%. Most sulfur is trapped by alunite precipitation that occurs in the 10 – 100 m distance range, with a peak volume fraction of 10%. Precipitation of these three minerals occurs mostly during the injection period (100 years), because the total SO_2 inventory is very small (1 wt% of CO_2 injected in the present simulation).

The zonal distribution of CO_2 and SO_2 trapping minerals reflects the pH distribution. CO_2 trapping minerals are stable in the higher pH ranges (above 5) beyond 100 m, and sulfur bearing minerals are stable in the low pH ranges (below 5) but not at extremely low pH values (0.6) in the 10 – 100 m radial zone.

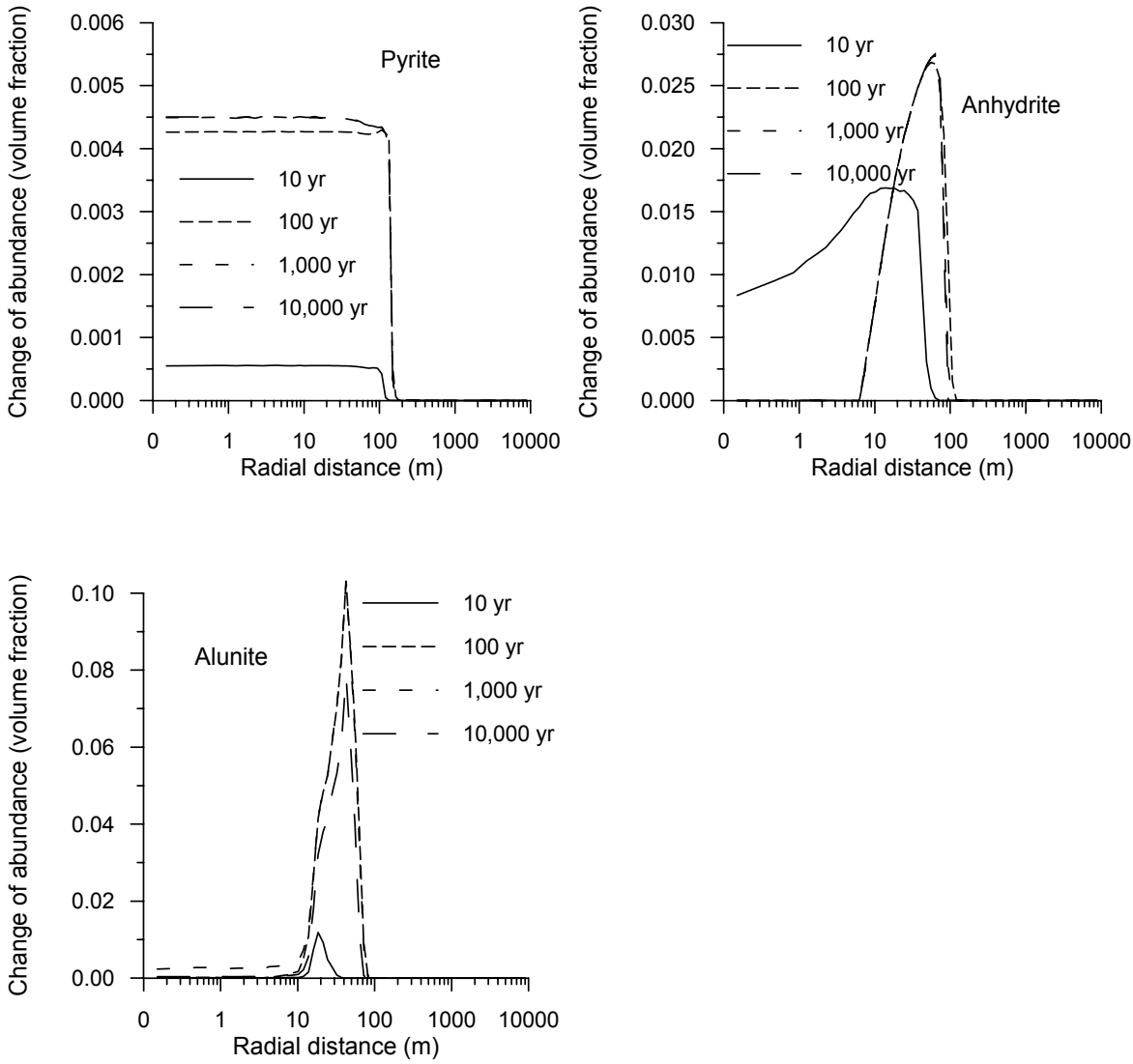

Figure 17. Change of mineral abundance for the case of injection of CO_2 with SO_2 (sandstone alone).

Injection of acid gases causes mineral alteration, resulting in significant changes in porosity (Figure 18), especially in the acidified zones where mineral dissolution dominates. With CO_2 + SO_2 injection, porosity in the acidified zone increases from an initial 0.3 to 0.52 after 100 years. In contrast, within the CO_2 mineral trapping zone, the porosity decreases to about 0.26 for both cases, because of the addition of CO_2 mass as secondary carbonates to the solid matrix. The precipitation of sulfur bearing minerals

causes the porosity to decrease to 0.25 at the 50 m from the well bore (Figure 18b). This location of minimum porosity coincides with the maximum precipitation of alunite (Figure 17c).

A small change in porosity can result in a significant change in permeability, which can modify fluid flow. The present simulations only monitor changes in porosity and permeability without feedback to the fluid flow. This feedback between flow and chemistry could be important and will be addressed in the future.

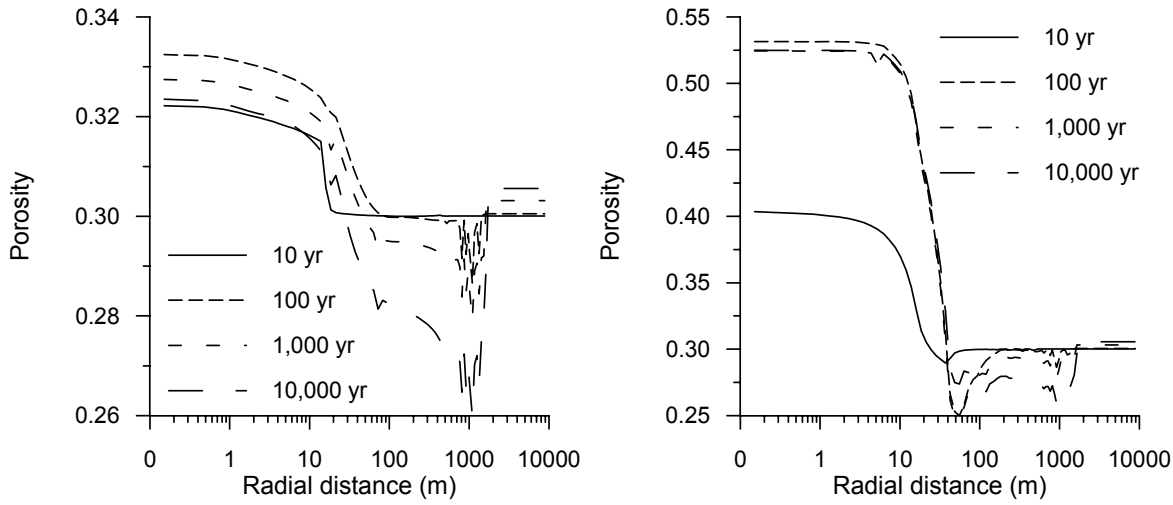

(a) CO_2 (b) CO_2+ SO_2

Figure 18. Porosity distribution at three different times.

4.2. Sandstone-shale system

Changes in mineral abundance, CO_2 sequestration, and porosity along sandstone horizon at different times are illustrated in Figures B.1 in Appendix B. The evolution of the variables in a vertical profile at a radial distance of 1000 m (in the CO_2 sequestration zone) are given in Figures B.2. Contour plots of some variables for the sandstone-shale system are shown in Figures B.3. Mineral alteration patterns (Figures B.1) are essentially similar to the results obtained by considering sandstone alone. This is because in the shale permeability is lower (Table 2) and diffusion is the dominant chemical transport

process. In the simulation time frame of 10,000 years, shale plays a limited role in mineral alteration and gas sequestration in the sandstone layer. Therefore, the system can be modeled by considering only sandstone for a short time period (less than 10,000 years). For natural diagenesis over periods of geological time, mass transfers between shale and sandstone are very important, as has been reported in Xu et al., (2004b) for a longer simulation period of 100,000 years.

5. Comparison of Simulations with Field Observations

Few mineralogical descriptions of the alteration of sandstone – shale sequences in the presence of high-pressure CO_2 are available in the literature that would allow comparison with the simulations presented in this paper. Those of interest usually reflect past accumulations of CO_2 associated with magmatic or volcanic activity. An example is that by Moore et al. (2003 and 2004), who describe the formation of secondary dawsonite and kaolinite in siltstones of the Permian Supai Formation of the Springerville-St. John CO_2 field on the border between Arizona and New Mexico. They observed secondary dawsonite spatially associated with corroded plagioclase and potassium feldspar, which is consistent with our simulations. Furthermore, their determination that kaolinite formed subsequent to dawsonite deposition following a decline in the CO_2 pressure, is also consistent with our finding that kaolinite is unstable during the precipitation of dawsonite. Authigenic illite appears to persist in the presence of dawsonite, which is also consistent with our modeling results. In contrast, the Supai Formation appears to have been more oxidizing, with a limited capacity to provide Fe^{+2} for the stabilization of ankerite.

Another recent paper (Watson et al., 2002) describes mineralogical and groundwater changes caused by magmatic carbon dioxide invading a gas reservoir in a lithic sandstone of the Pretty Hill Formation in the Ladbroke Grove gas field in South Australia. An important feature of this field example is that the mineralogy can be compared with an adjacent unmodified methane gas reservoir in the same formation. In contrast to those of the Supai Formation of Arizona and New Mexico, the conditions in this high-pressure CO_2 field are such that Fe^{+2} is available for the stabilization of siderite and ankerite. In this respect, the Ladbroke Grove field more closely represents the conditions of our simulation. Observed similarities include the destruction of chlorite in the lithic fragments and net corrosion of the feldspars, a reduction in the concentration of calcite, an increase in the concentration of siderite, a significant increase in the quantity of ankerite and a small increase in the quantity of quartz. However, no dawsonite was reported even though an evaluation of the coexisting groundwater indicates that it should

have been supersaturated with respect to this carbonate. A substantial increase in the concentration of kaolinite is observed, which is in conflict with our simulation. The porosity of the Ladbroke Grove reservoir also appears to have increased, whereas our simulation shows a decrease. The differences might be explained by the higher CO_2 pressure (201 vs. approximately 150 bar) and the higher Cl^- and Na^+ concentrations of the simulation.

Other field evidence suggests that magmatic CO_2 can also lead to the formation of dawsonite in arenaceous sedimentary formations, notably in the Bowen, Gunnedah and Sydney Basins of New South Wales (Baker et al., 1995), and the Denison Trough of east-central Queensland (Baker, 1991; Baker and Caritat, 1992). Dawsonite and kaolinite in these sedimentary accumulations appear to have been produced at the expense of detrital feldspars, in general agreement with the observations of Moore et al. (2003 and 2004). But it should be noted that feldspar destruction is incomplete, and on occasion, dawsonite is found in juxtaposition with unaltered feldspar (Loughnan and Goldbery, 1972). The field evidence is therefore suggestive of slow feldspar corrosion rates if not the eventual stabilization of feldspars. In these sedimentary formations, the occurrence of dawsonite is unrelated to the preceding precipitation or dissolution of diagenetic calcite, siderite and ankerite, which is attributed to early diagenesis and subsequent organic maturation (Baker, 1991).

Carbonate paragenesis in sedimentary formations invaded by magmatic CO_2 can vary in degree and complexity. The mineralogy, burial history, diagenesis, organic maturation, temperature and connate water salinity all play a role in addition to the timing and extent of magmatic CO_2 involvement. Thus it is hardly surprising that agreement between the present simulations and field observations is not perfect in all respects.

A number of simplifications related to SO_2 injection have been made, including (1) a limited suite of sulfate minerals anhydrite, gypsum and alunite that can precipitate from solution as a result of sulfuric acid generation and mineral dissolution, and (2) dissolved SO_2 instantly disproportionates into sulfuric acid and hydrogen sulfide. Detailed discussion regarding these simplifications is given in Appendix D.

6. Summary and Conclusions

We have developed a conceptual model of injection of CO_2 with H_2S and SO_2 in bedded sandstone-shale sequences using hydrogeologic properties and mineral compositions commonly encountered in Gulf Coast sediments. We have performed simulations of a 1-D radial well region considering sandstone alone, and a 2-D simulation considering a sandstone-shale sequence under acid-gas injection conditions. Major conclusions are as follows:

(1) In the simulation time frame of 10,000 years, shale adjacent to a sandstone horizon plays a limited role in mineral alteration and sequestration of gases. Therefore, the system can be essentially modeled by considering only sandstone. The reason is that permeability is lower in the shale and diffusion is the dominant chemical transport process. Nevertheless, for natural diagenesis over periods of geological time, mass transfers between shale and sandstone are very important.

(2) The co-injection of H_2S, compared to injection CO_2 alone, does not significantly affect pH distribution, the mineral alteration pattern, and CO_2 mineral sequestration. The co-injection of SO_2 results in a different pH distribution, and mineral alteration pattern.

(3) The zonal distribution of mineral alteration and formation of CO_2 and sulfur bearing minerals has been observed in the simulations, which reflects the pH distribution. With co-injection of SO_2, a larger (extended to 100 m radial distance over 20 m for CO_2 alone) and stronger (a lower pH of 0.6 over 3.4) acidified zone was obtained. Precipitation of CO_2 trapping minerals occurs in the higher pH regions beyond the acidified zones (CO_2 trapping zone). In contrast, sulfur bearing minerals are stable in the low pH ranges (below 5) but not extremely low pH values (0.6), which occur at radial distances ranging

from 10 – 100 m. Corrosion and well abandonment problems caused by SO_2 injection will be a very significant issue.

(4) For both CO_2 only and CO_2 + SO_2 cases, the patterns and amounts of carbonate mineral precipitation in CO_2 trapping zone are similar, except that the acidified zone resulting from injection of CO_2 only extends to a radial distance of 20 m from the well bore, whereas for co-injection of SO_2, it extends to 100 m. Significant CO_2 is sequestered in ankerite and dawsonite, and some in siderite. After 10,000 years, CO_2 mineral trapping can reach 76 kg per cubic meter of medium, which is very close to the maximum availability. The CO_2 trapping capability depends on the primary mineral composition. Precipitation of siderite and ankerite requires Fe^{2+} supplied by the dissolution of iron bearing minerals such as chlorite ($Mg_{2.5}Fe_{2.5}Al_2Si_3O_{10}(OH)_8$). Precipitation of dawsonite requires Na^+ provided by oligoclase ($CaNa_4Al_6Si_{14}O_{40}$) dissolution. The initial abundance of chlorite and oligoclase therefore affects the CO_2 mineral trapping capability.

(5) Most of sulfur is trapped by alunite precipitation, with a peak volume fraction of 10%, some by anhydrite, and a minor amount by pyrite. Pyrite also forms during co-injection of CO_2 and H_2S. Precipitation of these three sulfur-bearing minerals occurs primarily during the injection operation period (100 years), because the SO_2 inventory is very small (1 wt.% of CO_2 injected in the simulations).

(6) The addition of acid gases and the resulting mineral alteration leads to changes in porosity. Significant increases in porosity occur in the acidified zones where mineral dissolution dominates. With co-injection of SO_2, the porosity increases from an initial 0.3 to 0.52 after 100 years. However, within the CO_2 mineral trapping zone, the porosity decreases to about 0.26 for both cases, because of the addition of CO_2 mass as secondary carbonates to the rock matrix. The formation of sulfur bearing phases at the front of the acidified zone

causes porosity to decrease to 0.25. This location of minimum porosity coincides with the maximum precipitation of alunite. A small change in porosity can result in a significant change in permeability, which could modify fluid flow. This interaction between flow and chemistry could be important and will be addressed in the future.

(7) Limited information currently available for the mineralogy of natural high-pressure acid-gas reservoirs is also generally consistent with our simulation.

The range of problems concerning the interaction of water-gas-rock is very broad. The time needed to sequester acid gases in mineral phases is uncertain, because mineral kinetic properties and reactive surface areas are not well constrained. The present simulation results are specific to the conditions and parameters considered. The "numerical experiments" give a detailed understanding of the dynamic evolution of a geochemical system.

Acknowledgement. We thank Pat Dobson and Nicolas Spycher for reviews of the manuscript. This work was supported by the Director, Office of Science, Office of Basic Energy Sciences, of the U.S. Department of Energy, under Contract No. DE-AC03-76SF00098 with Lawrence Berkeley National Laboratory.

References

Ague, J.J., Brimhall, G.H., 1989. Geochemical modeling of steady state and chemical reaction during supergene enrichment of porphyry copper deposits. Economic Geology 84, 506-528.

Arnorson, S., Stefansson, A., 1999. Assessment of feldspar solubility constants in water in the range 0° to 350^oC at vapor saturation pressures. Am. J. Sci. 299, 173-209.

Bachu, S., Gunter, W.D., Perkins, E.H., 1994. Aquifer disposal of CO_2: hydrodynamic and mineral trapping. Energy Convers. Mgmt. 35, 269-279.

Bachu, S., Haug, K, Michael, K., Buschkuehle, B.E., and Adams, J. J., 2003, Deep Injection of Acid Gas in Western Canada, In Proceedings of Second International

Symposium on Underground Injection Science and Technology, October 22-25, 2003, Lawrence Berkeley National Laboratory, Berkeley, California

Baker, J.C., 1991. Diagenesis and reservoir quality of the Aldebaran Sandstone, Denison Trough, east-central Queensland, Australia. Sedimentology 38, 819-838.

Baker, J.C., Caritat, P., 1992. Postdepositional history of the Permian Sequence in the Denison Trough, Eastern Australia. Am. Assoc. Petrol. Geol. Bull. 76(8), 1224-1249.

Baker, J.C., Bai, G.P., Golding, S.D., Keene, J.B., 1995. Continental-scale magmatic carbon dioxide seepage recorded by dawsonite in the Bowen-Gunnedah-Sydney Basin system, Eastern Australia. J. Sed. Res. A65(3), 522-530.

Baroody, E.E., Carpenter, G.A., 1972. Heats of formation of propellant compounds (U), Rpt Naval Ordnance Systems Command task No. 331-003/067-1UR2402-001 for Naval Ordnance station, Indian Head, MD. 1-9 p.

Blum, A.E., Stillings, L.L., 1995. Feldspar dissolution kinetics, Chapter 7 of chemical weathering rates of silicate minerals, White, A.F., Brantley, S.L. (eds.), Mineral Society of America 31, 291–351, Washington D. C.

Corey, A. T., 1954, The interrelation between gas and oil relative permeabilities, Producers Monthly, 38 – 41.

Chou, L., Garrels R. M., and Wollast R., 1989. Comparative study of the kinetics and mechanisms of dissolution of carbonate minerals. *Chem. Geol.* 78, 269-282.

Devidal, J.L., Dandurand, J.L., Gout, R., 1996. Gibbs free energy of kaolinite from solubility measurement in basic solution between 60 and 170°C. Geochim. et Cosmochim. Acta 60(4), 553-564.

Ennis-King, J., and Paterson, L., 2003. Role of convective mixing of the long-term storage of carbon dioxide in deep saline formations, Paper SPE 84344, Presented at Society of Petroleum Engineers Annual Fall Technical Conference and Exhibition, Denver, CO, October 2003.

Ferrante, M.J., Stuve, J.M., Richardson, D.W., 1976. Thermodynamic data for synthetic dawsonite. U. S. Bureau of Mines Report of Investigations No. 8129, 13 pp.

García, J., Density of Aqueous Solutions of CO_2, Lawrence Berkeley National Laboratory Report LBNL-49023, Berkeley, CA, 2001.

Gautelier M., Oelkers E. H., and Schott J., 1999. An experimental study of dolomite dissolution rates as a function of pH from -0.5 to 5 and temperature from 25 to 80°C. *Chem. Geol.* 157, 13-26.

Gunter W.D., Perkins, E.H., McCann, T.J., 1993. Aquifer disposal of CO_2-rich gases: Reaction design for added capacity. Energy Convers. Mgmt. 34, 941-948.

Gunter W.D., Bachu, S., Law, D.H.S., Marwaha, V., Drysdale, D.L., MacDonald, D.E., McCann, T.J., 1996. Technical and economic feasibility of CO_2 disposal in aquifers within the Alberta Sedimentary Basin, Canada. Energy Convers. Mgmt. 37, 1135-1142.

Gunter, W.D., Perkins, E.H., Hutcheon, I., 2000, Aquifer disposal of acid gases: modelling of water–rock reactions for trapping of acid wastes. Applied Geochemistry, 15, 1085-1095.

Gunter W.D., Wiwchar, B., Perkins, E.H., 1997. Aquifer disposal of CO_2-rich greenhouse gases: extension of the time scale of experiment for CO_2-sequestering reactions by geochemical modeling. Mineral. and Petrol. 59, 121-140.

Helgeson, H.C., Kirkham, D.H., Flowers, G.C., 1981. Theoretical prediction of the thermodynamic behavior of aqueous electrolytes at high pressures and temperatures: IV. Calculation of activity coefficients, osmotic coefficients, and apparent molal and standard and relative partial molal properties to 600 C and 5 kb. Am. J. Sci. 281, 1249–1516.

Holloway, S., 1997, An overview of the underground disposal of carbon dioxide, *Energy Convers. Mgmt.*, 38, 193-198.

Johnson, J.W., Oelkers, E.H., Helgeson, H.C., 1992. SUPCRT92: A software package for calculating the standard molal thermodynamic properties of minerals, gases, aqueous species, and reactions from 1 to 5000 bars and 0 to 1000 degrees C. Computers and Geosciences 18, 899–947.

Johnson. J.W., Nitao, J.J., Steefel, C.I., Knaus, K.G., 2001. Reactive transport modeling of geologic CO_2 sequestration in saline aquifers: The influence of intra-aquifer shales and the relative effectiveness of structural, solubility, and mineral trapping during prograde and retrograde sequestration, In proceedings: First National Conference on Carbon Sequestration. Washington, DC.

Kaszuba, J.P., Janecky, D.R., Snow, M.G., 2003, Carbon dioxide reaction processes in a model brine aquifer at 200 °C and 200 bars: implications for geologic sequestration of carbon. Applied Geochemistry, 18, 1065-1080.

Knauss, K. G., Steefel, C. I., Johnson, J. W., Boram, L. H., 2002. Impact of CO_2, contaminant gas, aqueous fluid, and reservoir rock interactions on the geologic sequestration of CO_2, Geological Society of America Annual Meeting, Session 135 (13), October 27-30, Denver, Colorado.

Korbol, R., Kaddour, A., 1995. Sleipner vest CO_2 disposal - injection of removed CO_2 into the Utsira Formation. Energy Convers. Mgmt. 36 (6-9), 509-512.

Kreitler, C.W., Richter, B.C., 1986. Hydrochemical characterization of saline aquifers of the Texas Gulf Coast used for the disposal of industrial waste. Report to the US Environmental protection Agency under Cooperative agreement No. CR821786-01-0. University of Texas at Austin, Bureau of Economic Geology.

Kusakabe. M., Komoda, Y., Takano, B., Abiko, T., 2000, Sulfur isotopic effects in the disproportionation reaction of sulfur dioxide in hydrothermal fluids: implications for the $\delta^{34}S$ variations of dissolved bisulfate and elemental sulfur from active crater lakes. Journal of Volcanology and Geothermal Research, v. 97, p. 287-307.

Kulik, D.A., Aja, S.U., 1997 (July 20-24). Hydrothermal stability of illite: implications of empirical correlations and Gibbs Energy minimization. Proceedings on the Fifth International Symposium on Hydrothermal Reactions, Gatlinburg, Tennessee, 228-292.

Land, L.S., Mack, L.E., Milliken, K.L., Lynch, F.L., 1997. Burial diagenesis of argillaceous sediment, south Texas Gulf of Mexico sedimentary basin: A reexamination. GSA Bulletin 109(1), 2-15.

Lasaga, A.C., 1984. Chemical kinetics of water-rock interactions, J. Geophys. Res. 89, 4009-4025.

Law, D.H.S., Bachu, S., 1996. Hydrogeological and numerical analysis of CO_2 disposal in deep aquifers in the Alberta Sedimentary Basin. Energy Convers. Mgmt. 37(6-8), 1167 - 1174.

Lohuis, J.A.O., 1993. Carbon dioxide disposal and sustainable development in The Netherlands, Energy Convers. Mgmt. 34(9-11), 815-821.

Malmstrom M., Banwart S., Lewenhagen J., Duro L., and Bruno J., 1996. The dissolution of biotite and chlorite at 25ºC in the near-neutral pH region. *Contaminant Hydrology,* 21, 201-213.

McPherson, B.J.O.L., Lichtner, P.C., 2001. CO_2 sequestration in deep aquifers, In proceedings: First National Conference on Carbon Sequestration. Washington, DC.

Moore, J., Adams, M., Allis, R., Lutz, S., Rauzi, S., 2003. CO_2 mobility in natural reservoirs beneath the Colorado Plateau and Southern Rocky Mountains: An example from the Springerville-St. Johns field, Arizona and New Mexico, In proceedings: Second National Conference on Carbon Sequestration, May 2003, Washington, DC.

Moore, J., Adams, M., Allis, R., Lutz, S., Rauzi, S., 2004. Mineralogical and geochemical consequences of the long term presence of CO_2 in natural reservoirs: An example from the Springerville-St. Johns field, Arizona and New Mexico, USA. Submitted to Chemical Geology.

Nagy, K.L., 1995. Dissolution and precipitation kinetics of sheet silicates, Chemical Weathering Rates of Silicate Minerals 31, 291–351.

Nagy K. L., Cygan R. T., Hanchar J. H., and Sturchio N. C., 1999. Gibbsite growth kinetics on gibbsite, kaolinite, and muscovite substrates: Atomic force microscopy evidence for epitaxy and an assessment of reactive surface area. *Geochim. Cosmochim. Acta,* 63(16), 2337-2351.

Narasimhan, T.N., Witherspoon, P.A., 1976. An integrated finite difference method for analyzing fluid flow in porous media, Water Resour. Res. 12, 57–64.

Nordstrom, D.K., Muñoz, J.L., 1986. Geochemical Thermodynamics, The Benjamin/Cummings Pub. Co., Menlo Park, California, 477 pp.

Oelkers, E. H., Pokrovsky, O., Schott, J., 2002. An experimental study of magnesite dissolution and precipitation rates, 2002 Geological Society of America, Session 135 (1), October 27-30, Denver, Colorado.

Ortoleva, P.J., Dove, P., Richter, F., 1998 (May 10-12). Geochemical perspectives on CO_2 sequestration, Manuscript prepared for U. S. Department of Energy Workshop on "Terrestrial Sequestration of CO_2 - An Assessment of Research Needs," Gaithersburg, MD.

Palandri, J. L., Kharaka, Y. K., 2002. Adding kinetics to equilibrium-based geochemical

modeling of CO_2 sequestration, 2002 Geological Society of America Annual Meeting, Session 174 (5), October 27-30, Denver, Colorado.

Parkhurst, D.L., Thorstenson, D.C., Plummer, L.N., 1980. PHREEQE: A computer program for geochemical calculations: US Geological Survey, Water Resources Investigation 80-96, 174 pp.

Pearce, J.M., Holloway, S., Wacker, H., Nelis, M.K., Rochelle, C., Bateman, K., 1996. Natural occurrences as analogues for the geological disposal of carbon dioxide. Energy Convers. Mgmt. 37 (6-8), 1123-1128.

Perkins, E.H., Gunter, W.D., 1995. A users manual for PATHARC.94: a reaction path-mass transfer program, Alberta Research Council Report ENVTR 95-11, 179 pp., Canada.

Perkins, E. H., Gunter, W.D., Hutcheon, I., Shevalier, M., Durocher, K., Emberley, S., 2002. Geochemical modelling and monitoring of CO_2 storage at the Weyburn site, Saskatchewan, Canada, 2002 Geological Society of America Annual Meeting, Session 174 (11), October 27-30, Denver, Colorado.

Pruess, K., Oldenburg, C., Moridis, G., 1999. TOUGH2 user's guide, Version 2.0. Lawrence Berkeley Laboratory Report LBL-43134, Berkeley, California.

Pruess, K., Xu, T., Apps, J., García, J., 2003. Numerical modeling of aquifer disposal of CO_2. SPE (Society of Petroleum Engineers) Journal, p. 49-59, March (2003).

Reed, M.H., 1982. Calculation of multicomponent chemical equilibria and reaction processes in systems involving minerals, gases and aqueous phase. Geochim. Cosmochim. Acta 46, 513-528.

Rimstidt, J.D., 1997. Quartz solubility at low temperatures. Geochim. Cosmochim. Acta 61, 2553-2558.

Rochelle, C.A., Bateman, K., Pearce, J.M., 1996. Fluid-rock interactions resulting from the underground disposal of carbon dioxide, In Bottrell, S. H. (ed.), Proc., 4th lnt. Symp. Geochem, Earth's Surf.. University of Leeds, Dep. of Earth Sciences, Leeds, UK., 448-452.

Shock, E.L., Sassani, D.C., Willis, M., Sverjensky, D.A., 1997. Inorganic species in geologic fluids, Correlations among standard molal thermodynamic properties of aqueous ions and hydroxide complexes. Geochim. Cosmochim. Acta 61, 907-950.

Sonnenthal, E.L., Spycher, N., 2001. Drift-Scale coupled processes (DST and THC seepage) models. AMR N0120/U0110 Rev.01, Yucca Mountain Project, Lawrence Berkeley National Laboratory, Berkeley, California.

Soong, Y., Goodman, A.L., McCarthy-Jones, J.R., Baltrus, J.P., 2004, Experimental and simulation studies on mineral trapping of CO_2 with brine. Energy Conversion and Management, 45, 1845-1859.

Steefel, C.I., van Cappellen, P., 1990. A new kinetic approach to modeling water-rock interaction: The role of nucleation, precursors and Ostwald ripening. Geochim. Cosmochim. Acta 54, 2657-2677.

Steefel, C.I., Lasaga, A.C., 1994. A coupled model for transport of multiple chemical species and kinetic precipitation/dissolution reactions with applications to reactive flow in single phase hydrothermal system. Am. J. Sci. 294, 529-592.

Steefel C. I., 2001. CRUNCH, Lawrence Livermore National Laboratory, pp. 76.

Strazisar, B. R., Zhu, C., 2002. One-dimensional reactive transport model for geological carbon sequestration, 2002 Geological Society of America Annual Meeting, Session 174 (6), October 27-30, Denver, Colorado.

Stumm, W., Morgan, J.J., 1981. Aquatic chemistry: An introduction emphasizing chemical equilibria in natural waters. 780 pp., John Wiley & Sons, New York.

Tester, J.W., Worley, G.W., Robinson, B.A., Grigsby, C.O., Feerer, J.L., 1994. Correlating quartz dissolution kinetics in pure water from 25° to 625 °C., Geochim. et Cosmochim. Acta 58, 2407–2420.

van Genuchten, M. Th., 1980, A Closed-form equation for predicting the hydraulic conductivity of unsaturated soils, Soil Sci. Soc. Am. J. 44, 892 – 898.

Watson, M.N., Zwingmann, N., Lemon, N.M., 2002 (October 1-4). The Ladbroke Grove-Katnook carbon dioxide natural laboratory: A recent CO_2 accumulation in a lithic sandstone reservoir. Extended Abstract E1-5, Siixth International Conference on Greenhouse Gas Control Technologies (GHCT-6), Kyoto, Japan, 6 p.

Weir, G. J., S. P. White, and W. M. Kissling, Reservoir Storage and Containment of Greenhouse Gases, in: K. Pruess (ed.), *Proceedings of the TOUGH Workshop '95*, Lawrence Berkeley National Laboratory Report LBL-37200, p. 233-238, Berkeley, CA, 1995.

White, S.P., Weir, G. J., Kissling, W.M., 2001(May 14-17). Numerical simulation of CO_2 sequestration in natural CO_2 reservoirs on the Colorado Plateau. In Proceedings of First National Conference on Carbon Sequestration, Washington, DC.

Wolery, T.J., 1992. EQ3/6: Software package for geochemical modeling of aqueous systems: Package overview and installation guide (version 7.0). Lawrence Livermore National Laboratory Report UCRL-MA-110662 PT I, Livermore, California.

Xu, T., Pruess, K., 2001. Modeling multiphase non-isothermal fluid flow and reactive geochemical transport in variably saturated fractured rocks: 1. Methodology. Am. J. Sci., 301, 16-33.

Xu, T, Apps, J.A., Pruess, K., 2003. Reactive geochemical transport simulation to study mineral trapping for CO_2 disposal in deep arenaceous formations, Journal of Geophysical Research 108(B2).

Xu, T, Apps, J.A., Pruess, K., 2004a. Numerical simulation to study mineral trapping for CO_2 disposal in deep aquifers, Applied Geochemistry, 19, 917-936.

Xu, T, Apps, J.A., Pruess, K., 2004b. Mineral sequestration of carbon dioxide in a sandstone-shale system, Submitted to "Chemical Geology".

Xu, T., Sonnenthal, E.L., Spycher, N., and Pruess, K., 2004c, TOUGHREACT user's guide: A simulation program for non-isothermal multiphase reactive geochemical transport in variable saturated geologic media, Lawrence Berkeley National Laboratory Report LBNL-55460, Berkeley, California. pp. 192.

Yeh, G.T., Tripathi, V.S., 1991. A model for simulating transport of reactive multispecies components: model development and demonstration. Water Resour. Res. 27, 3075-3094.

Appendix A. Time Evolution at 1.25 and 1000 m from the Injection Well Considering Sandstone Alone

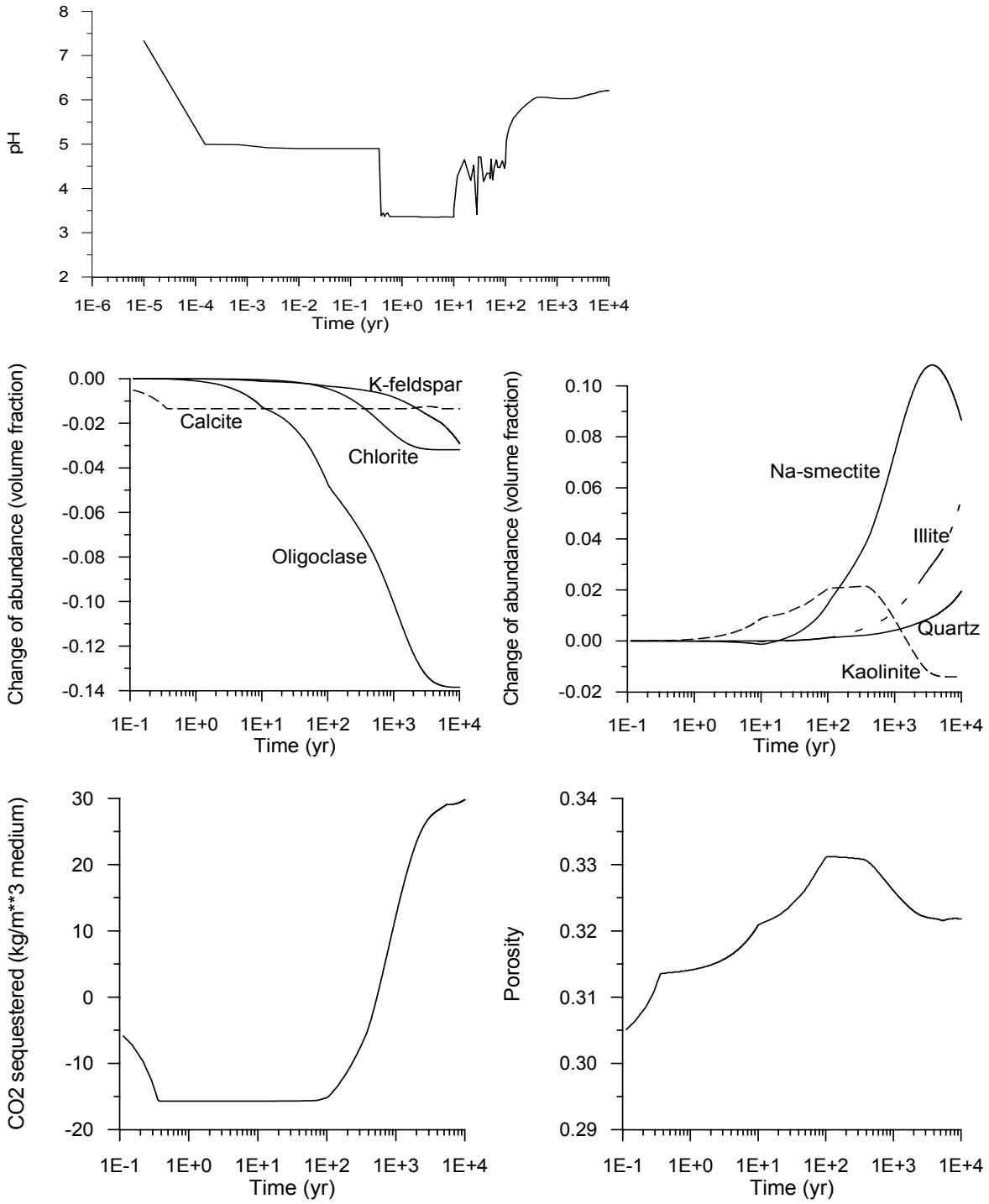

Figure A.1. Time evolution at 1.25 m for CO_2 only case.

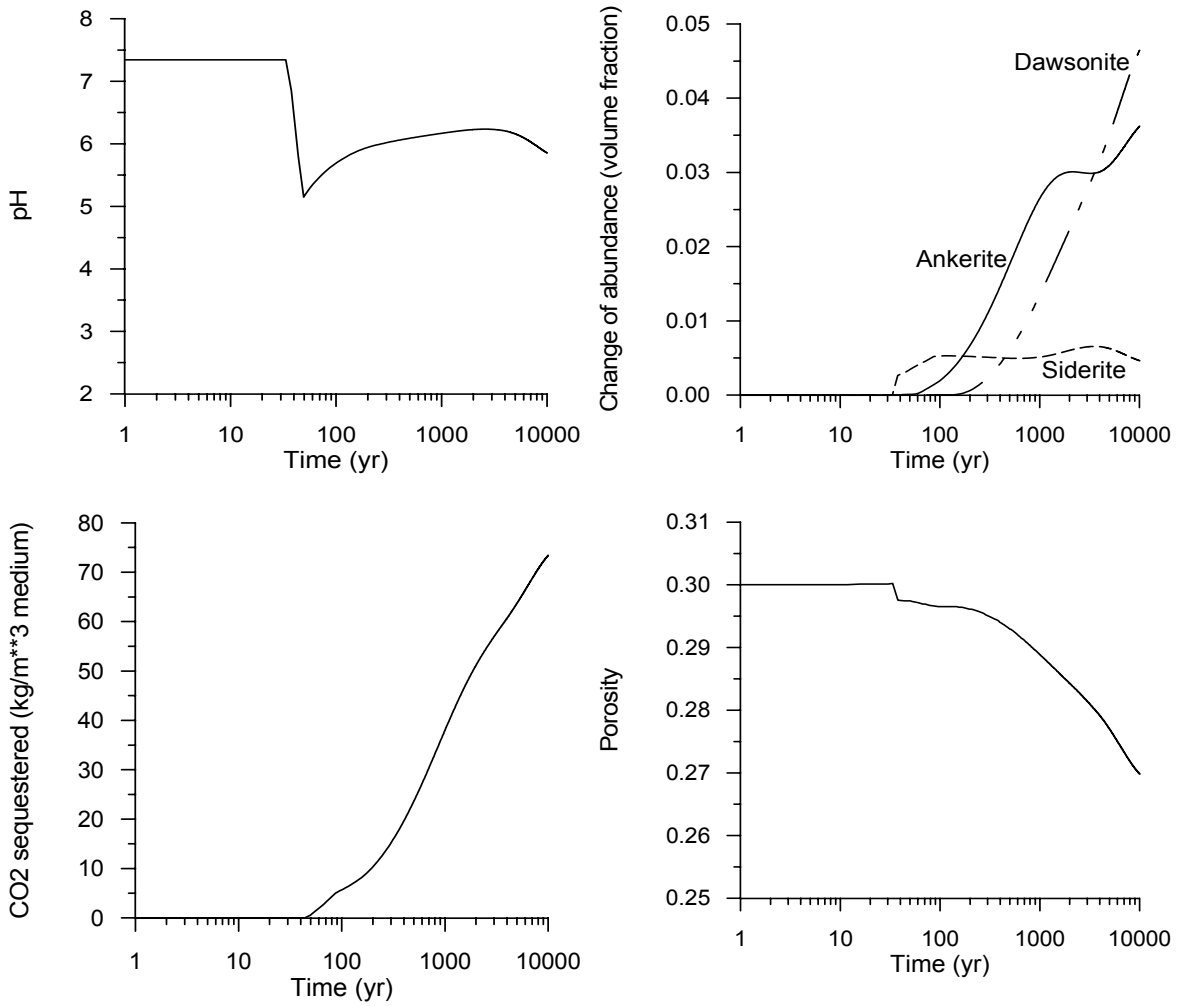

Figure A.2. Time evolution at 1000 m for CO_2 only case.

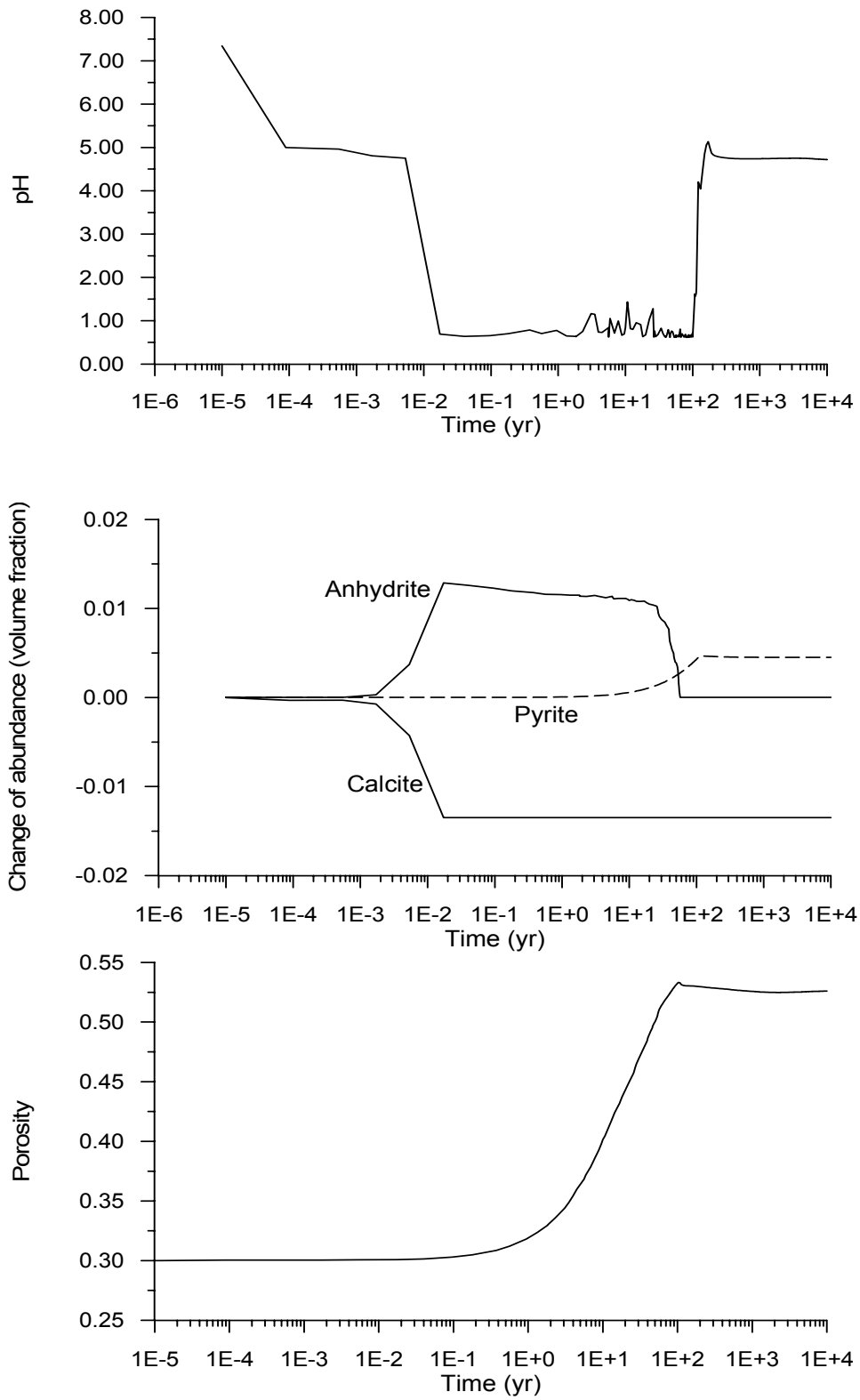

Figure A.3. Time evolution at 1.25 m for CO_2 + SO_2 case.

Appendix B. Results along sandstone horizon obtained from the sandstone-shale system

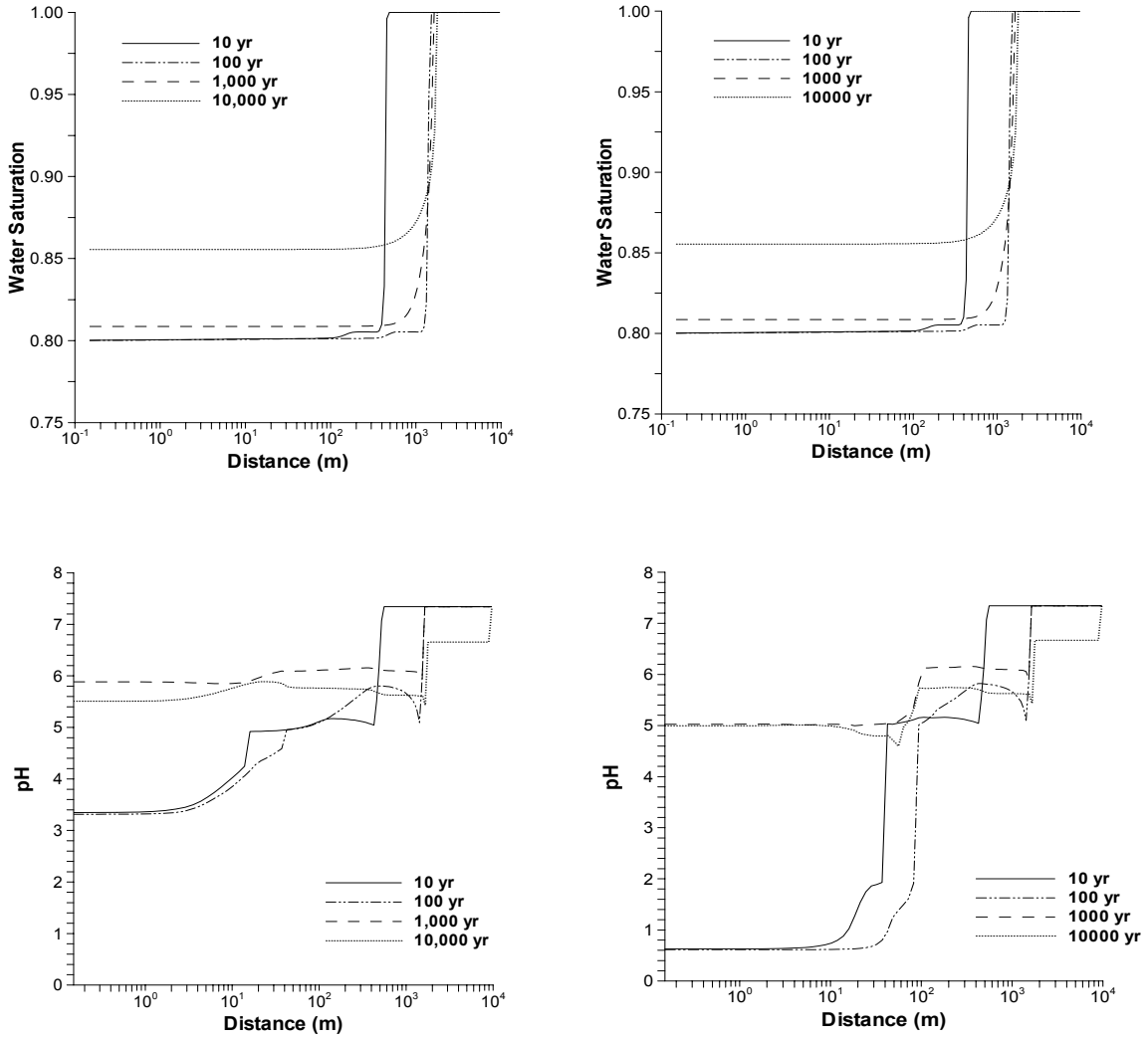

CO_2 only

CO_2 with SO_2

Figure B.1-1. Results along sandstone horizon at different times. The left column is for injection CO_2 only, and the right column for injection CO_2 with SO_2.

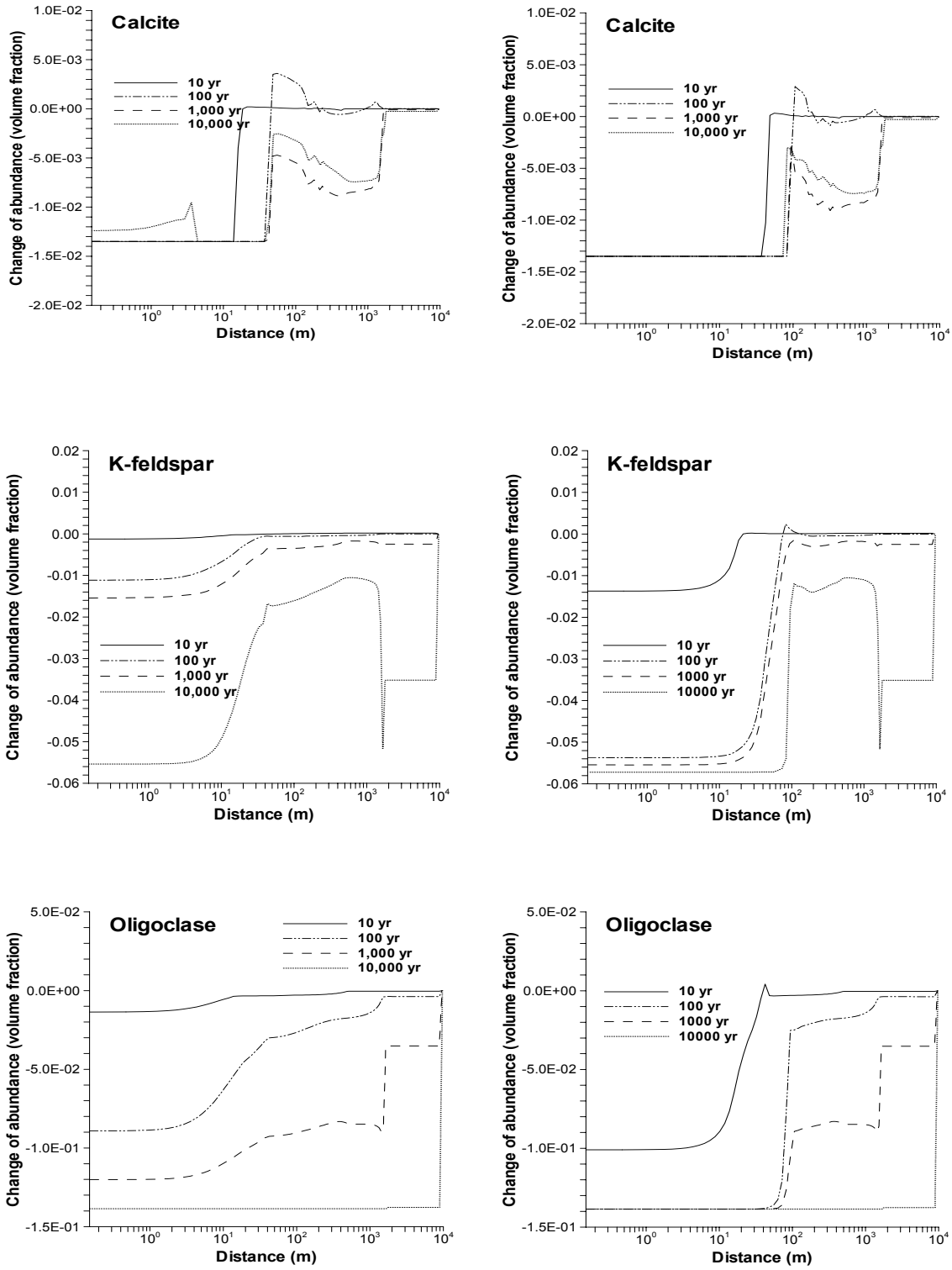

CO_2 only

CO_2 with SO_2

Figure B.1-2. Results along sandstone horizon at different times.

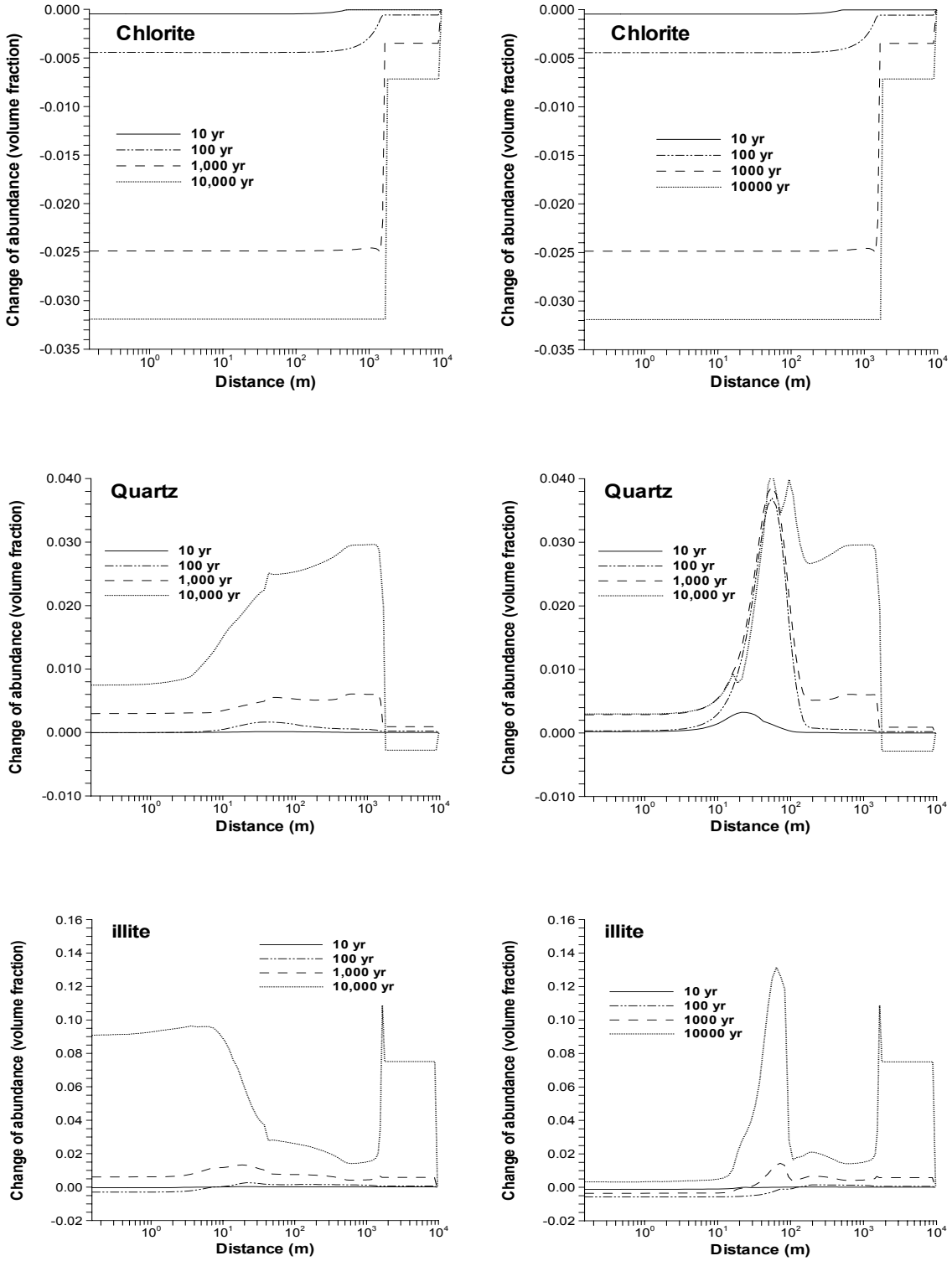

CO_2 only CO_2 with SO_2

Figure B.1-3. Results along sandstone horizon at different times.

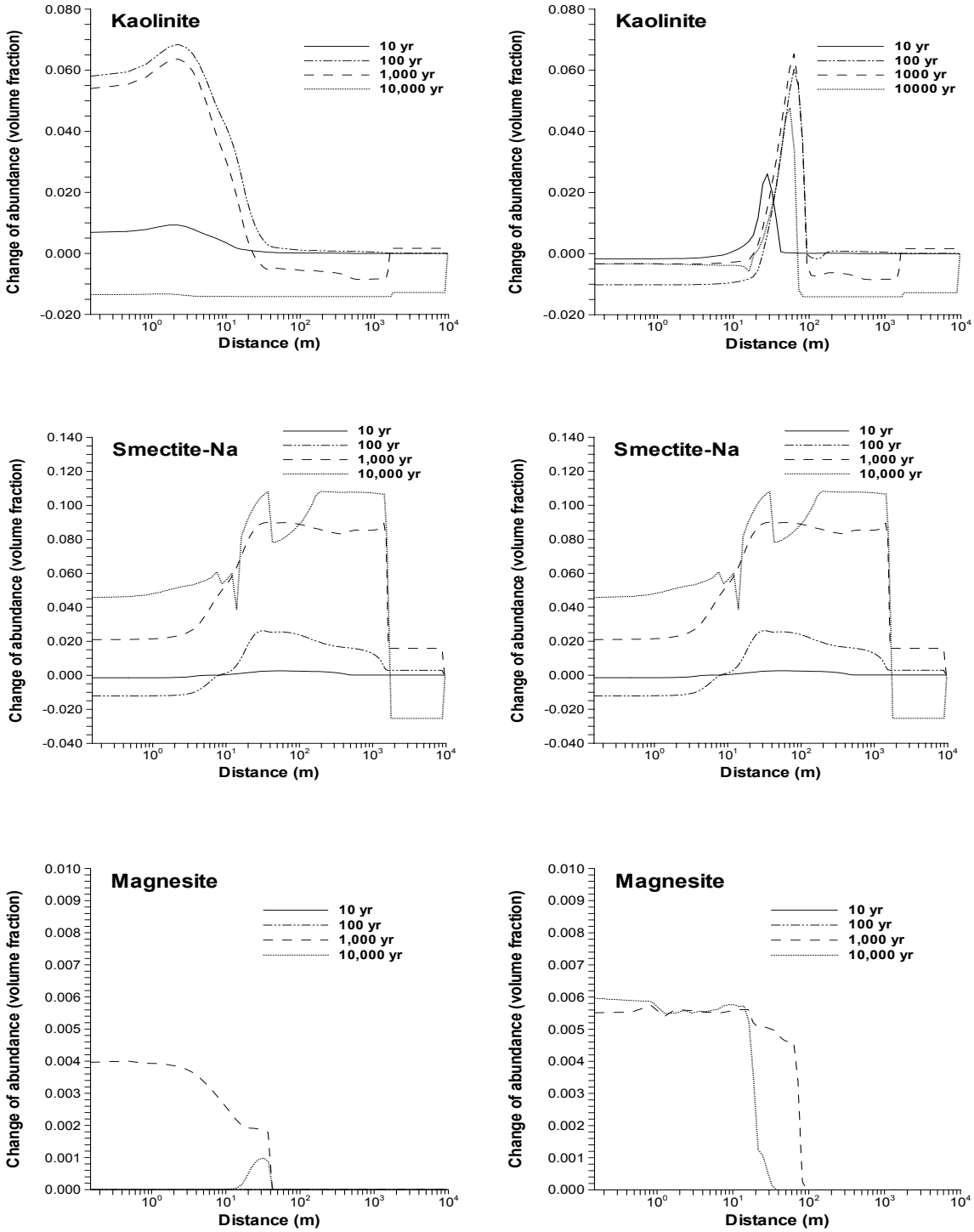

CO_2 only CO_2 with SO_2

Figure B.1-4. Results along sandstone horizon at different times.

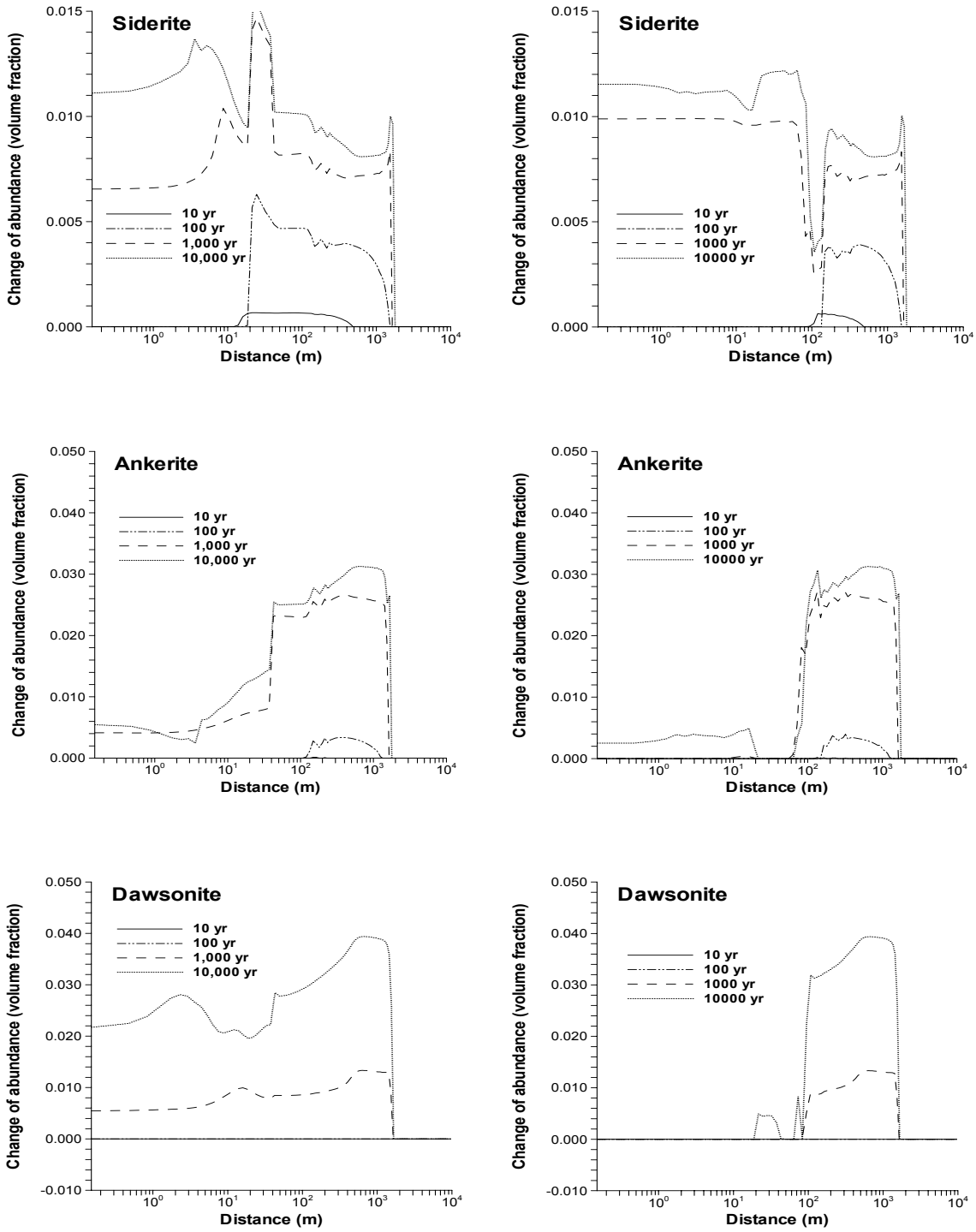

CO_2 only CO_2 with SO_2

Figure B.1-5. Results along sandstone horizon at different times.

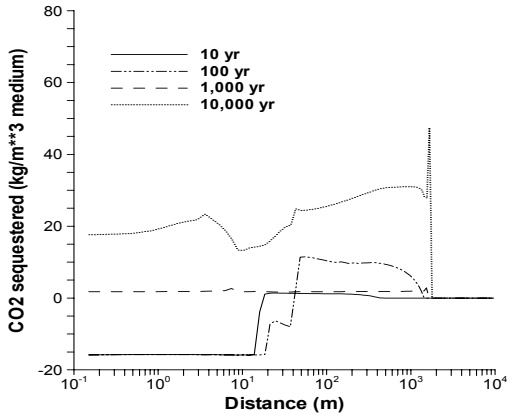

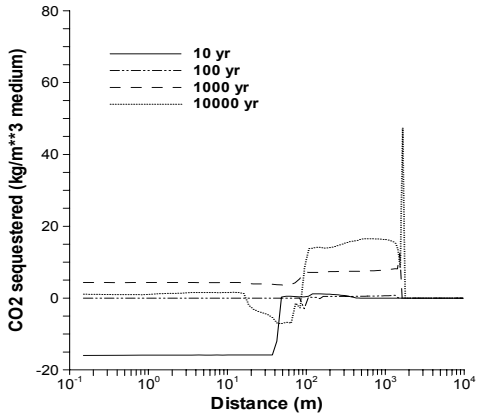

No pyrite in SO_2-free system

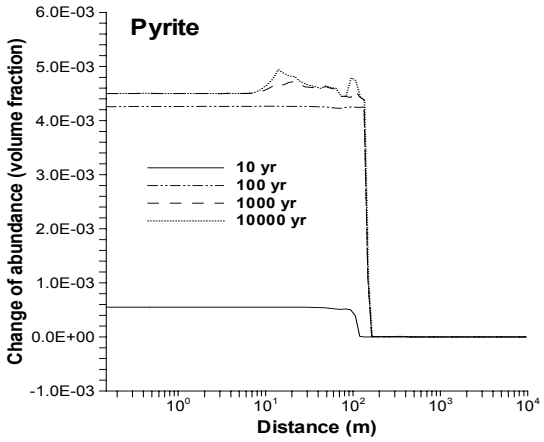

No anhydrite in SO_2-free system

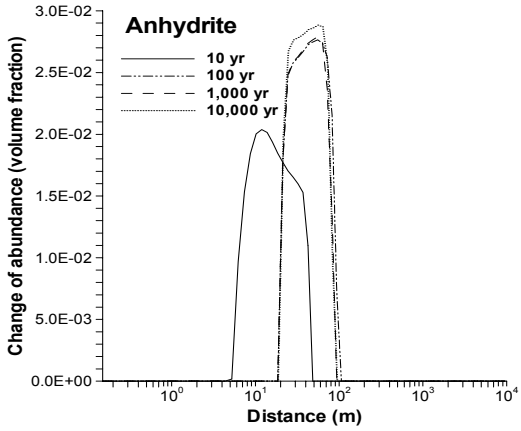

CO_2 only

CO_2 with SO_2

Figure B.1-6. Results along sandstone horizon at different times.

No alunite in SO_2-free system

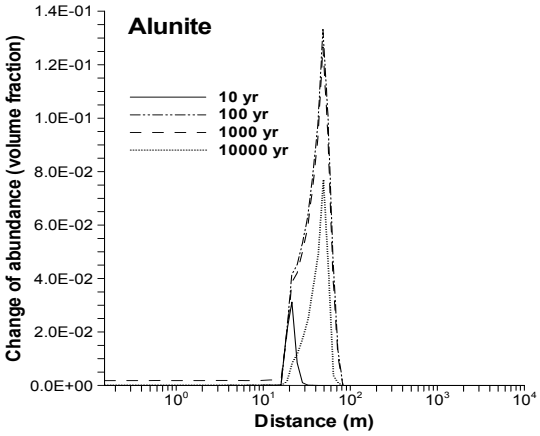

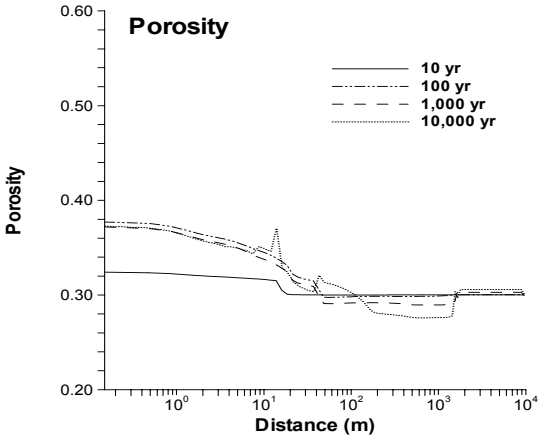

CO_2 only

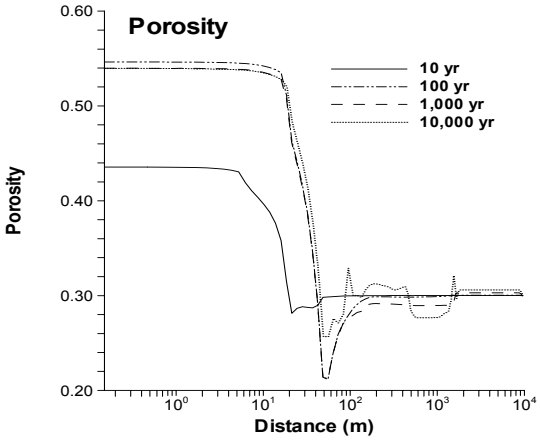

CO_2 with SO_2

Figure B.1-7. Results along sandstone horizon at different times.

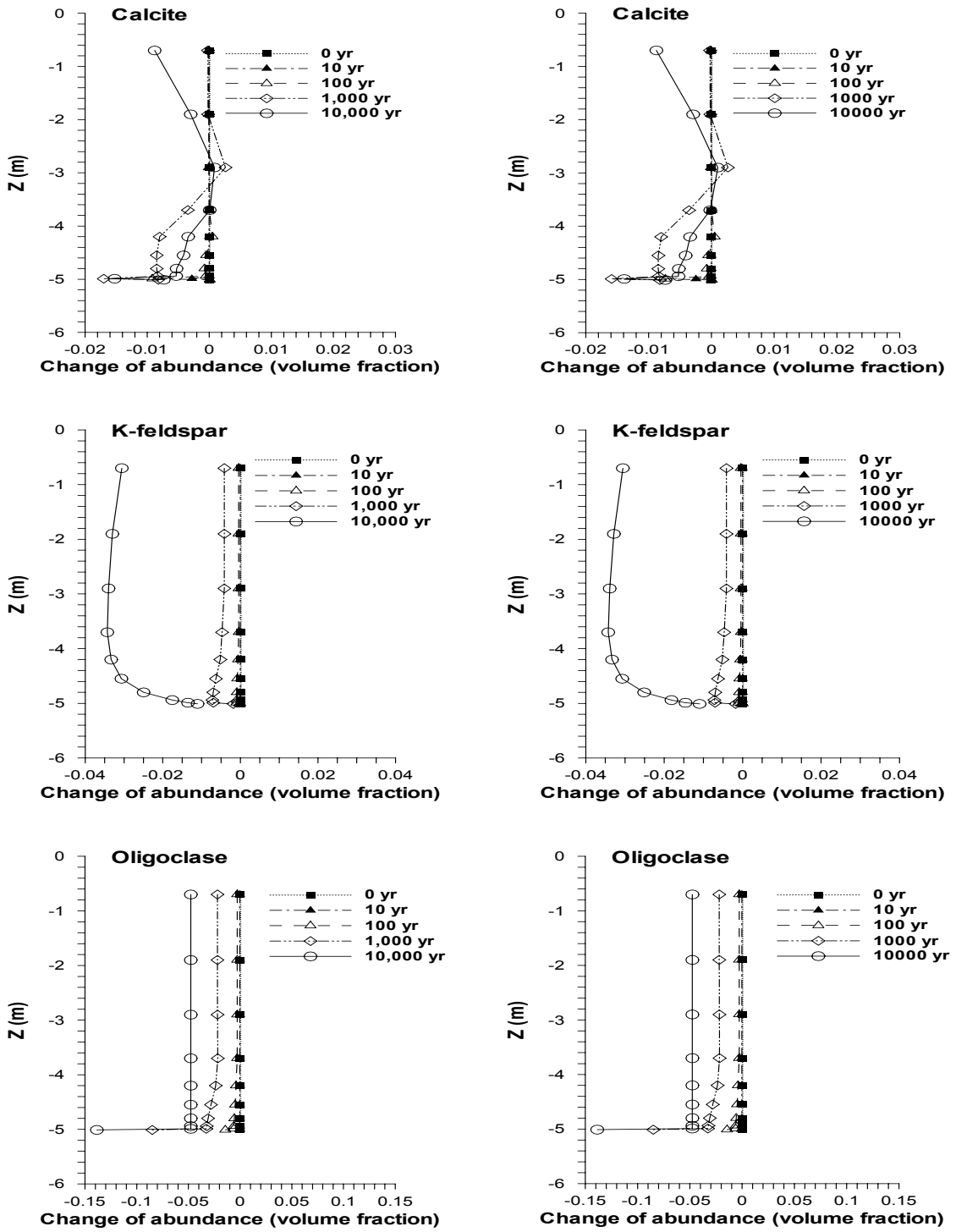

CO_2 only CO_2 with SO_2

Figure B.2-1. Results along vertical profile at 1000 m radial distance (the bottom grid block is for sandstone).

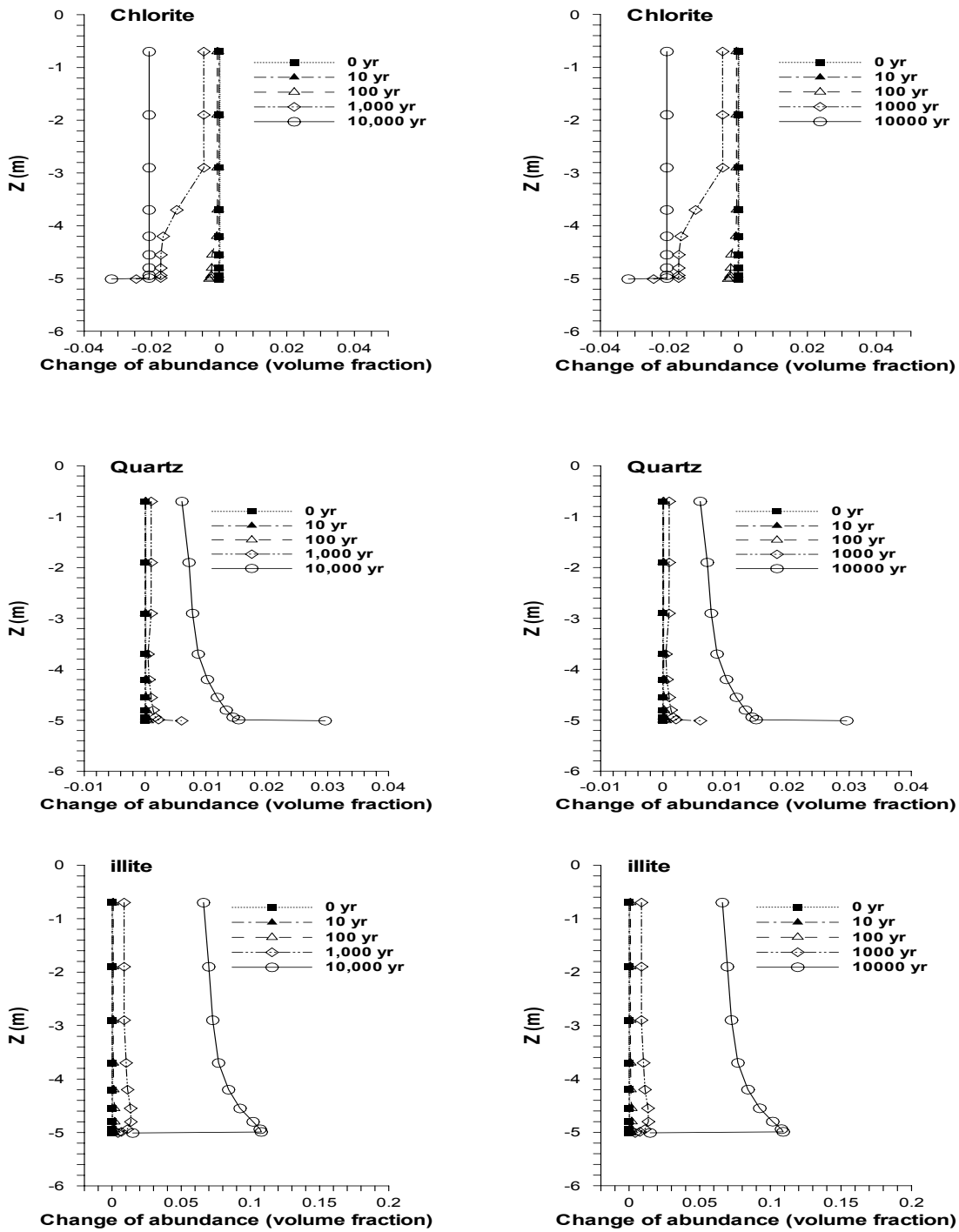

CO_2 only

CO_2 with SO_2

Figure B.2-2. Results along vertical profile at 1000 m radial distance.

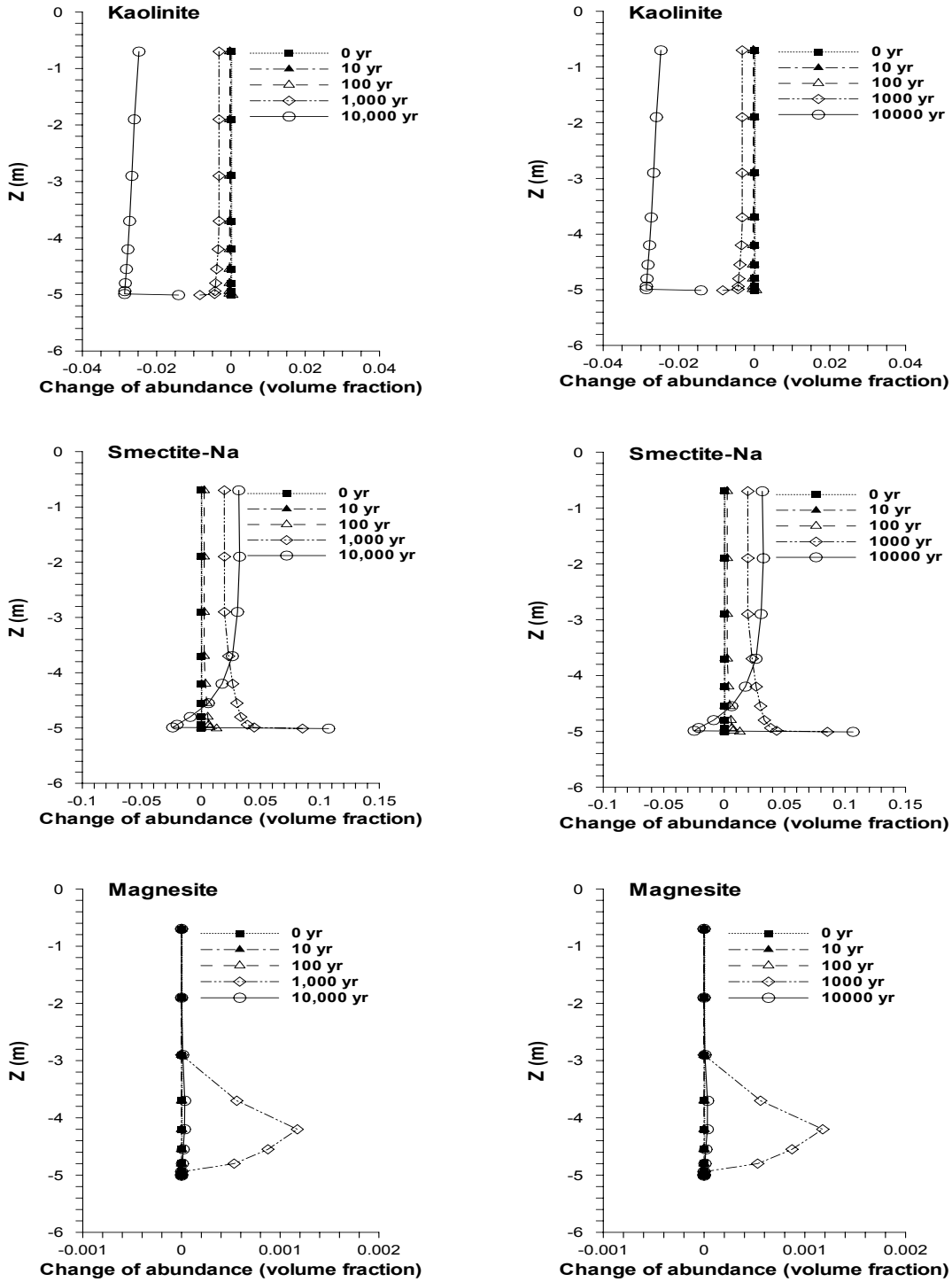

CO_2 only

CO_2 with SO_2

Figure B.2-3. Results along vertical profile at 1000 m radial distance.

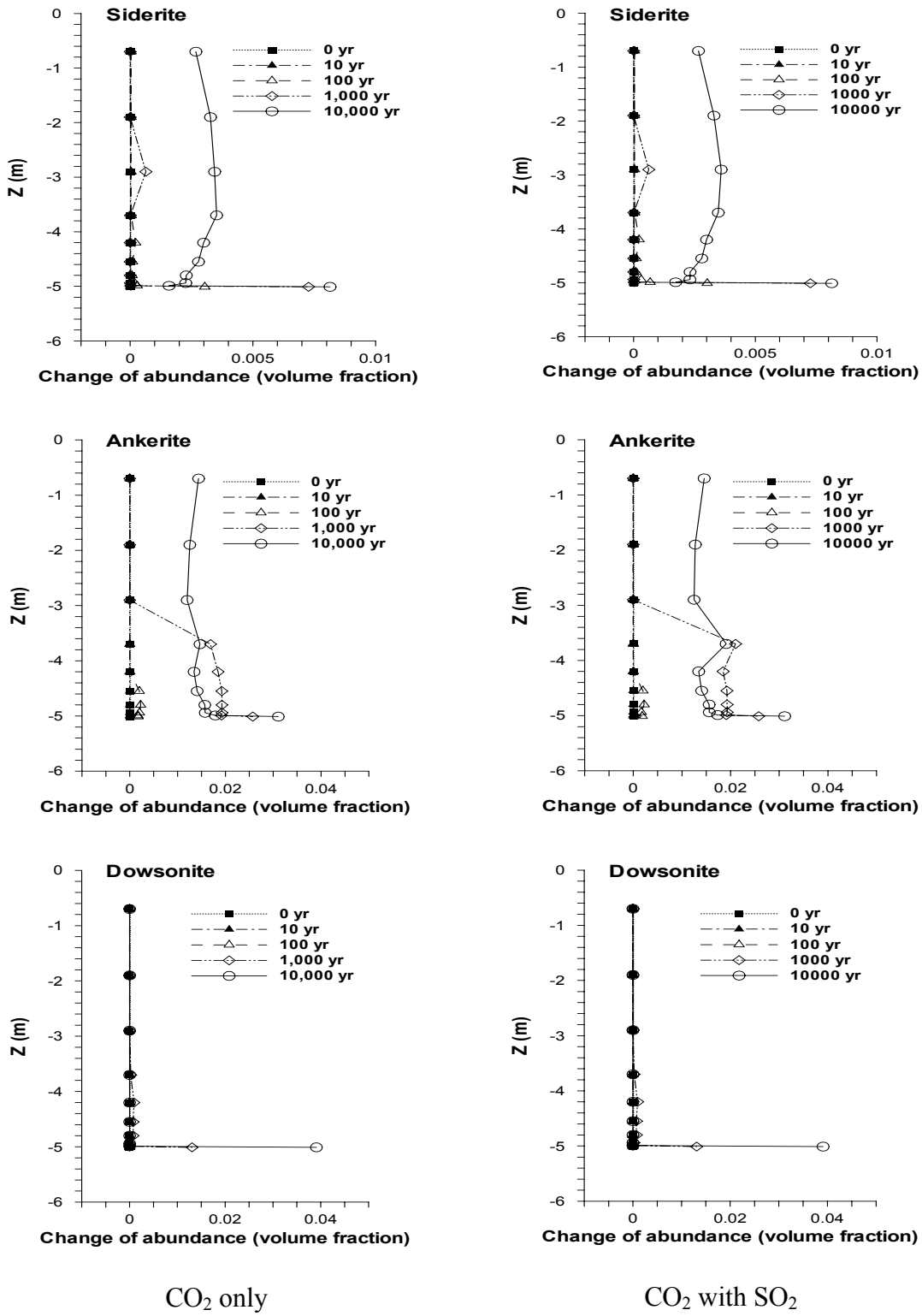

Figure B.2-4. Results along vertical profile at 1000 m radial distance.

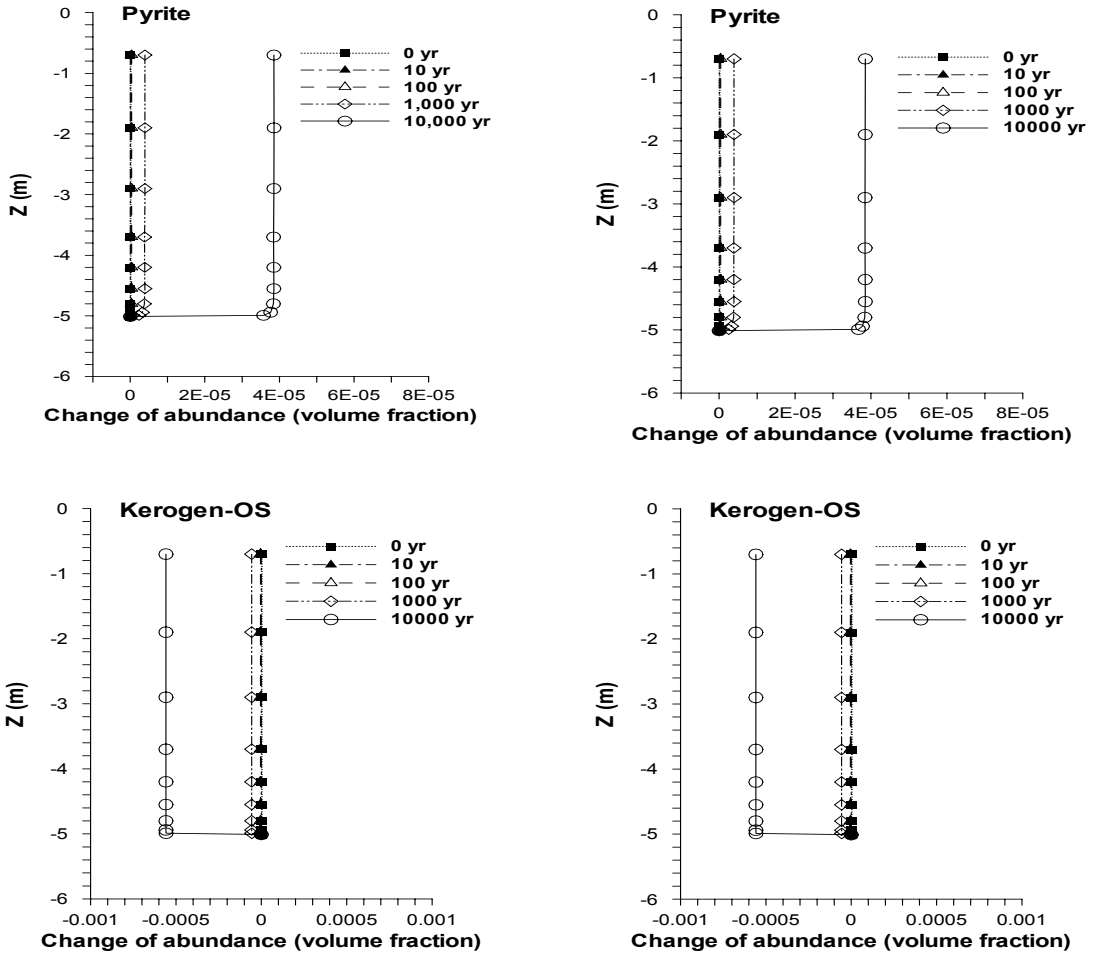

CO_2 only

CO_2 with SO_2

Figure B.2-5. Results along vertical profile at 1000 m radial distance.

Appendix C. Results (contour plot) obtained from the sandstone-shale system

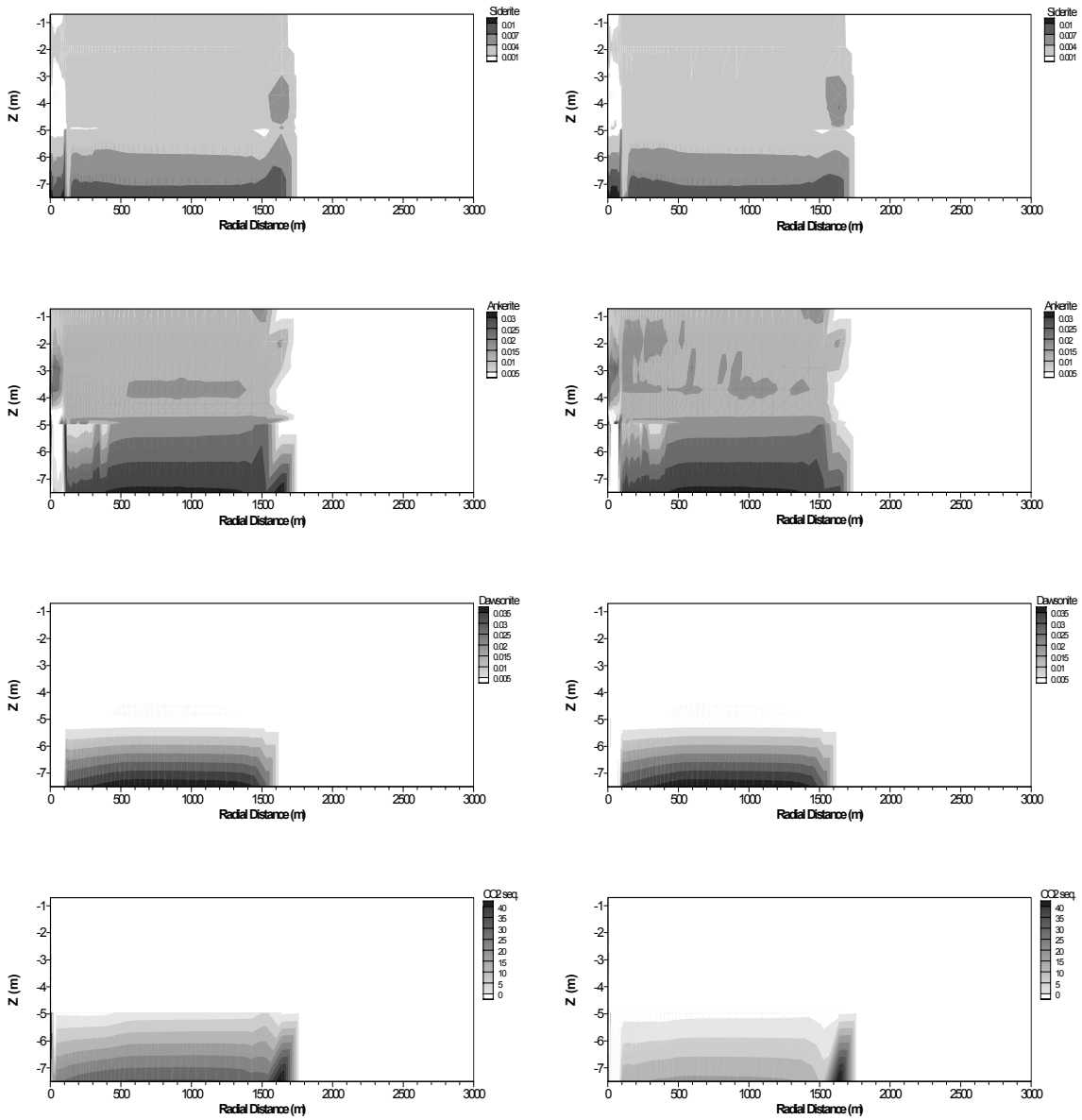

CO_2 only CO_2 with SO_2

Figure C.1-1. Contour plot after 10,000 years for the sandstone-shale system.

No pyrite in SO_2-free system

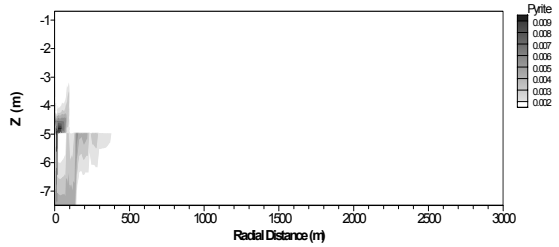

No anhydrite in SO_2-free system

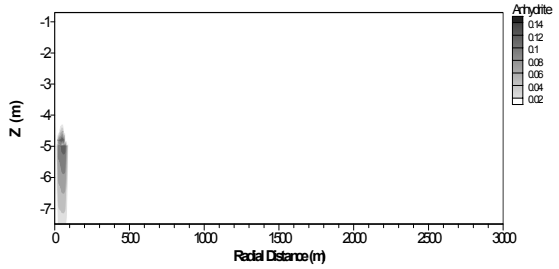

No alunite in SO_2-free system

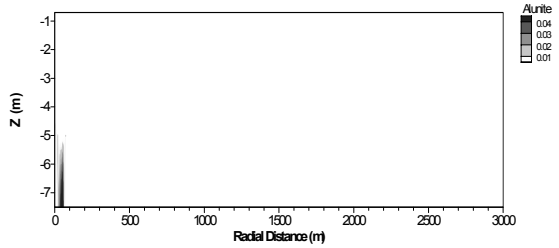

CO_2 only

CO_2 with SO_2

Figure C.1-2. Contour plot after 10,000 years for the sandstone-shale system.

Appendix D. Discussion on simplified treatments in current modeling related to SO_2 injection

D.1. Discussion of Current Limitations

Research to address the current limitations is outlined below.

Thermodynamic Properties of Sulfate Phases

The extremely acid conditions generated through the disproportionation of SO_2 in the aqueous phase, and consequent formation of sulfuric acid, would induce dissolution of aluminosilicate minerals. The excess silica would initially precipitate as amorphous silica, and the solubilized alumina would precipitate as secondary basic aluminum sulfates, some of which could be amorphous or poorly crystalline. Table D.1 summarizes some of the principal aluminum sulfate phases that are most commonly observed in natural systems, and are likely to precipitate under the conditions currently being modeled. Early attempts to characterize phases in the system Al_2O_3-SO_3-H_2O include the investigations by Bassett and Goodwin (1949), mainly at 25°C, but with some studies at 50 and 70°C, and Henry and King (1949, 1950) at 60°C. Subsequently, Nordstrom (1982) conducted a thorough review of the literature up to that time, and quantified the solubility products of several important aluminum sulfates including basaluminite, jurbanite and alunogen. Because of slow crystallization kinetics, many phases in the system are metastable. Nordstrom particularly emphasized the importance of the metastable persistence of basaluminite, and jurbanite in relation to alunite. However, he did not attempt to evaluate the solubility products of basic aluminum sulfates incorporating alkali metal and alkali earth cations such as halotrichite, pickeringite, tamarugite and mendozite. Furthermore, although Nordstrom's evaluation was excellent for its time, he relied on aqueous aluminum species thermodynamic properties that have been substantially revised since, e.g. see Pokrovskii et al, (1995), Shock et al. (1997) and Tagirov and Schott (2001). His data would not, therefore, be suitable for current modeling without substantial revision.

Table D.1. Status of Thermodynamic Properties of Secondary Phases that could participate in the Modeled System

Mineral name	Formula	ΔG^o_f	ΔH^o_f	S^o	$C_p(T)$	Solubility Sources
Sulfites						
Hannebachite	$CaSO_3.0.5H_2O$					See text
Orschallite	$Ca_3(SO_3)_2(SO_4).12H_2O$		See text			
Sulfates						
Bassanite	$CaSO_4.0.5H_2O$					EQ3/6 data0.dat
Felsobanyaite	$Al_4(SO_4)(OH)_{10}.5H_2O$					
Basaluminite	$Al_4(SO_4)(OH)_{10.}5H_2O$					Singh (1969) Singh and Brydon (1969) Adams and Rawajfih (1977)
Hydrobasaluminite	$Al_4(SO_4)(OH)_{10}.12\text{-}36H_2O$					
Zaherite	$Al1_2(SO_4)_5(OH)_{26}.20H_2O$					
Aluminite	$Al_2(SO_4)(OH)_4.7H_2O$					
Meta-aluminite	$Al_2(SO_4)(OH)_4.5H_2O$					
Jurbanite	$Al(SO_4)(OH).5H_2O$					Nordstrom (1982)
Alunogen	$Al_2(SO_4)_3.17H_2O$					Nordstrom (1982)
Alunite	$KAl_3(OH)_6(SO_4)_2$		Kelley et al. (1946)	Kelley et al. (1946)	Kelley et al. (1946)	Adams and Rawajfih (1977) Nordstrom (1982)
Halotrichite	$FeAl_2(SO_4)_4.22H_2O$					
Pickeringite	$MgAl_2(SO_4)_4.22H_2O$					
Tamarugite	$NaAl(SO_4)_2.6H_2O$					
Mendozite	$NaAl(SO_4)_2.11H_2O$					

Thermodynamic Properties of Sulfite Phases

The two most important naturally occurring sulfites, which should be incorporated in future modeling activities, are hannebachite ($CaSO_3.0.5H_2O$) and orschallite ($Ca_3(SO_3)_2(SO_4).12H_2O$). $CaSO_3$ can substitute as $CaSO_3.2H_2O$ into gypsum $CaSO_4.2H_2O$, and form a partial solid solution series (Setoyama and Takahashi, 1978, 1979; Takahashi and Setoyama, 1982). Similarly, $CaSO_4.0.5H_2O$ can substitute into the $CaSO_3.0.5H_2O$ structure up to a mol fraction of at least 0.12 (Jones et al., 1977a,b). Orschallite is also observed to form a partial solid solution series $Ca_3(SO_3)_x(SO_4)_{(3-x)}.12H_2O$, where $1 \leq x \leq 3$ (Zangen and Cohen, 1985; Cohn and Zangen, 1985). The cited authors conducted thermogravimetric analysis and differential scanning calorimetry on discrete members of the solid solution.

An extensive literature exists on the solubility of $CaSO_3.0.5H_2O$ in sulfurous acid solutions at various temperatures. Most of the earlier literature is summarized by Lutz (1986), and includes notable contributions by Schwartz and Muller-Clemm (1921), Ghurd et al. (1935), Gishler and Maass (1935a,b), Otuka (1939a,b), Frydman et al. (1958), Nilsson et al. (1958), Rengamo et al. (1958), Engelhardt (1962), Templeton et al. (1963) and Rodin and Margules (1983a,b). A very precise determination of the solubility of $CaSO_3.0.5H_2O$ at 25°C was published subsequently by Rai et al. (1991). Studies have also been conducted to measure the solubility of $CaSO_3.0.5H_2O$ in sucrose solutions including those by Gupta et al. (1965), Bobrovnik and Kotel'nikova (1974) and Malghe and Kumar (1998).

A critical evaluation of the data contained within these literature sources in conjunction with appropriate data drawn from specific aqueous speciation studies, e.g. Frydman et al. (1958), Nilsson et al. (1958), Rengamo et al. (1958), and Rai et al. (1991), should permit satisfactory data to be obtained for the thermodynamic properties of hannebachite. An evaluation of information provided on the partial solid solution series between gypsum and $CaSO_3.2H_2O$ by Setoyama and Takahashi (1978, 1979) and Takahashi and Setoyama (1982), and the partial solid solution between hannebachite and $CaSO_4.0.5H_2O$ by Jones et al. (1977a,b) might also allow for the formulation of appropriate solid solution models to predict precipitation behavior in aqueous sulfite – sulfate solution mixtures. Finally, the limited thermogravimetric analyses and differential scanning calorimetry by Zangen and Cohen (1985) and Cohen and Zangen (1985) might be used to construct an approximate solid solution model for orschallite.

Thermodynamic Characterization of Sulfite species in the Aqueous Phase, and Modeling of Sulfite solutions of High Ionic Strength

In general, the temperature dependent thermodynamic properties of the most common aqueous sulfite species i.e. $SO_2(aq)$, HSO_3^-, and SO_3^{--}, are well established. However, the properties of postulated complexes are less well known. Rai et al. (1991) have determined the $\log K^o = 2.62 \pm 0.07$ for formation of the ion pair $CaSO_3(aq)$. Information on other potentially significant species, i.e. $NaSO_3^-$, $NaHSO_3(aq)$, $MgSO_3(aq)$, $MgHSO_3^+$ and $CaHSO_3^+$ do not appear to be available in the literature, although some information on these species might be recovered from published experimental data involving multi-component aqueous systems containing sulfite.

Rai et al (1991) also evaluated the Pitzer ion interaction coefficients for Na^+ - SO_3^{2-} and Ca^{2+} - SO_3^{2-}at 25°C, although they preferred to represent the latter explicitly through the formation of a strongly bound ion pair. The modeling of concentrated sulfite solutions using Pitzer interaction theory would be preferable in the analysis of $CaSO_3.0.5H_2O$ solubility data.

Kinetics of Sulfur Dioxide Disproportionation in the Aqueous Phase

Current simulations assume the instantaneous interaction of SO_2 with the aqueous phase to produce thermodynamically more stable products, as represented by the following disproportionation equation:

$$4SO_2 + 4H_2O = 3SO_4^{--} + 6H^+ + H_2S(aq)$$

This means that the dissolved SO_2 is immediately converted into sulfuric acid and hydrogen sulfide without the opportunity for the SO_2 as sulfurous acid to interact with the host rock primary and secondary minerals and precipitate secondary sulfites.

This problem can be resolved through modification of the TOUGHREACT code to permit the incorporation of the kinetics of homogeneous reactions within the aqueous phase. The TOUGHREACT code has been modified accordingly, but incorporation of SO_2 disproportionation kinetics has not yet been implemented in the current project.

A search of the literature has yielded very little useful information that would allow for the quantitative modeling of the sulfite disproportionation in the aqueous phase according to equation (1). It is unlikely that experiments to define the rate of reaction

would be easily accomplished; as sulfur intermediates are likely to form with intermediate oxidation states, e.g. see Druschel, et al. (2003). The reaction could also be catalyzed by transition metal cations, which would be present in any natural system, e.g. see Kraft and Van Eldik (1989).

Ryabinina and Oshman (1972) investigated the thermal decomposition of aqueous H_2SO_3 at 120 – 140°C and found the reaction to be autocatalytic with an $S_2O_3^{2-}$ intermediate product. The activation energy for the reaction was 21.28 kcal/mol. Rempel et al. (1974) reported on the decomposition kinetics of 0.51-5.20 *M* $NaHSO_3$ aqueous solutions in an autoclave at 110-180°C and with pH values between 2 and 5. The process was apparently autocatalytic with a $(S_2O_3.SO_2)^{2-}$ intermediate. The effective activation energy of 16.5 kcal/mol was reported. Khorunzhii et al. (1984) investigated the kinetics of disproportionation of sulfur dioxide in hydrochloric acid solutions, but no further information is given in the citation.

Kinetics of Dissolution or Precipitation of Hydroxy-aluminosulfate Phases

Nordstrom (1982) and others, e.g. Boudot et al. (1996) have emphasized the tendency for hydroxy-aluminosulfates to precipitate from solution as poorly crystalline or amorphous solids, which subsequently transform to crystalline solids. Many soil solutions equilibrate with respect to metastable phases, such as basaluminite or jurbanite (Nordstrom, 1982) with consequent elevation of the aluminum species in solution (Boudot et al., 1996). This example of the Ostwald rule of Stages shows that coexisting solution compositions are determined by kinetic, rather than thermodynamic considerations. For realistic simulations of the reaction of sulfuric acid with host-rock aluminosilicates, and precipitation of secondary aluminosulfates, it is important that the kinetics of precipitation and dissolution of this class of phases is incorporated in the model. Unfortunately, much of the literature on the system Al_2O_3-SO_3-H_2O describes phase transformations only in a qualitative sense. Therefore, only approximations of the rate constants could be derived from such data. However, even if such ill-defined constants were incorporated in the model, this would constitute a substantial improvement over models where such data is omitted entirely.

Kinetics of Dissolution or Precipitation of $CaSO_3.0.5H_2O$

Tseng (1984) conducted a definitive study of the dissolution and precipitation kinetics of $CaSO_3.0.5H_2O$ in fulfillment of his requirements for a Ph.D. Tseng developed an integrated mass transfer model incorporating solution equilibrium to predict $CaSO_3.0.5H_2O$ dissolution rates as a function of pH, solution composition, temperature, and particle size. Both dissolution and crystallization were inhibited by dissolved sulfate. The rate of crystal growth in terms of BET surface area, mol/cm^2.min, was given as

$$R' = 9.7 \times 10^{-4} \exp(-10250/RT) \times (RS_{CaSO3} - 1)^2 \times RS_{CaSO4}^{-1}$$

where RS_{CaSO3} and RS_{CaSO4} are the relative saturations with respect to $CaSO_3.0.5H_2O$ and $CaSO_4.2H_2O$, respectively. Tseng also determined that $CaSO_3.0.5H_2O$ contained sulfate in solid solution, when precipitated from solution containing dissolved sulfate, in conformity with the findings of Jones et al. (1977a,b). The growth rate of $CaSO_3.0.5H_2O$ from solution was also determined in a later study by Tai and Chen (1995). These

investigators found that the rate of precipitation followed a parabolic rate law involving σ, the relative supersaturation:

$$R_g = k\sigma^n$$

where $k = 3.68 \times 10^{-9}$ mol/cm^2.min, and $n = 2.26$. Tai and Chen (1995) showed that their results were consistent with those of Tseng and Rochelle (1986).

D.2. Summary of Proposed Research Activities

The following tasks are recommended in meeting the goal of a more accurate simulation of acid gas injection containing SO_2

(1) Review and evaluate available information pertaining to the disproportionation of SO_2 in the aqueous phase. Incorporate the reaction rate constants in the version of TOUGHREACT designed to incorporate homogeneous reaction kinetics.
(2) Evaluate the literature relating to the solubility of hannebachite in the aqueous phase as a function of temperature. Derive appropriate temperature dependent solubility products. Evaluate orschallite thermodynamic properties and estimate temperature dependent solubility products.
(3) Evaluate the dissolution and precipitation rate data for hannebachite from published literature. Estimate the corresponding rate data for orschallite.
(4) Update temperature dependent solubility product data for alunite, jurbanite, basaluminite and alunogen, using revised aluminum speciation data.
(5) Estimate the kinetics of precipitation of hydroxy-aluminosulfate phases as a function of temperature.
(6) Develop a kinetic model for describing the Ostwald Rule of Stages with respect to silica and hydroxy-aluminosulfate phases. Modify TOUGHREACT to account for sequential precipitation and dissolution of metastable phases.
(7) Evaluate solid solution models of the hannebachite-bassanite series and the gypsum- $CaSO_3.2H_2O$ series. Modify TOUGHREACT to account for solid solutions.

D.3. References

Adams, F. and Hajek, B.F., 1978. Effects of solution sulfate, hydroxide, and potassium concentrations on the crystallization of alunite, basaluminite, and gibbsite from dilute aluminum solutions. Soil Science, v. 126(3), p. 169-173.

Adams, F. and Rawajfih, Z., 1977. Basaluminite and alunite: a possible cause of sulfate retention by acid soils. Soil Sci. Amer. Proc., v.41, p. 686-692.

Bassett, H. and Goodwin, T.H., 1949. The basic aluminum sulfates. J. Chem. Soc., p. 2239-2279.

Bobrovnik, L.D. and Kotel'nikova, L.P., 1974. Solubility of calcium sulfite in sugar solutions [in Russian]. Izvestiya Vysshikh Uchebnykh Zavedenii, Pishchevaya Teckhnologiya, No. 4, p. 155-156.

Boudot, J.-P., Maitat, Q., Merlet, D. and Rouiller, J., 1996. Occurrence of non-monomeric species of aluminum in undersaturated soil and surface waters:

consequences for the determination of mineral saturation indices. Journal of hydrology, v. 177, p. 47-63

Cohen, A., and Zangen, M., 1985. Studies on alkaline earth sulfites – VIII. Thermal behaviour of $Ca_3(SO_3)_2(SO_4).12H_2O$ and its solid solution in calcium sulfite tetrahydrate and crystallographic data on dehydrated salts. Revue de Chimie Minerale, v. 22, p. 427-436.

Druschel, G.K., Hamers, R.J. and Banfield, J.F., 2003. Kinetics and mechanism of polythionate oxidation to sulfate at low pH by O_2 and Fe^{3+}. Geochim. et Cosmochim. Acta, v. 67(23), p. 4457-4469.

Engelhardt, G., 1962. Physikalisch-chemische probleme der bisulfitkochsauren. Zellstoff und Papier (Leipzig), v. 11(2), p. 43-50.

Frydman, M., Nilsson, G., Rengamo, T. and Sillen. L.G., 1958. Solution equilibriums involving calcium sulfite and carbonate. III. Acidity constants of H_2CO_3 and H_2SO_3, and $CaCO_3$ + $CaSO_3$ equilibrium in $NaClO_4$ medium at 25C^o. Acta Chemica Scandinavica, v. 12, p. 878-884.

Ghurd, G.W., Gishler, P.E. and Maass, O., 1935a. Studies on the system calcium oxide – sulfur dioxide –water: 1. Determination of the vapor pressure and conductivities. Canadian Journal of Research, v. 13, (B), p.209-217.

Gishler, P.E. and Maass, O., 1935b. Studies on the system calcium oxide – sulfur dioxide –water: 1I. Calculations of ionic concentrations. Canadian Journal of Research, V. 13, (B), p. 308-322.

Gishler, P.E. and Maass, O., 1935. Studies on the system calcium oxide – sulfur dioxide –water: 1II. Precipitation temperatures. Canadian Journal of Research, V. 13, (B), p.370-379.

Gupta, S.C., Ramaich, N.A. and Kumar, K., 1965. Studies on the solubility of calcium sulfite in sugar solutions. Proc. Ann. Conv. Sugar Technologist's Assoc. India, v. 33(2), p. 175-179.

Henry, J.L. and King, G.B., 1949. The system aluminum sulfate-sulfuric acid-water at 60C^o. . J. Amer. Chem. Soc., v. 71, p. 1142-1144.

Henry, J.L. and King, G.B., 1950. Phase rule investigation of the system Al_2O_3-SO_3-H_2O at 60C^o, basic region. . J. Amer. Chem. Soc., v. 72, p. 1282-1286.

Jones, B.F., Philip, S., and Meserole, F.B., 1977. Experimental and theoretical studies of solid solution formation in lime and limestone sulfur dioxide scrubbers, Volume 1. Final report. Radian Corp., Austin, Texas, USA. U.S. NTIS, PB Rep., 75 p.

Jones, B.F., Lowell, P.S. and Meserole, F.B., 1977. Experimental and theoretical studies of solid solution formation in lime and limestone sulfur dioxide scrubbers, Volume 1I. Appendices. Radian Corp., Austin, Texas, USA. U.S. NTIS, PB Rep., 75 p.

Khorunzhii, B.I., Volodin, N.I., Zakharov, Yu.D. and Fateeva, V.P., 1984. Kinetics of disproportionation of sulfur dioxide in hydrochloric acid solutions [in Russian]. Khimiya i Tekhnol.Monomerov, M., p. 25-30. CA 103-221785.1984

Kraft, J. and Van Eldik, R., 1989. Kinetics and mechanism of iron(III)-catalyzed autoxidation of sulfur(IV) oxides in aqueous solution. 2. decomposition of transient iron(III)-sulfur(IV) complexes. Inorganic Chemistry, v. 28(12), p. 2306-2312.

Lutz, H.D., 1986. Calcium Sulfite. In Sulfites, selenites and tellurites (Kertes, A.S. ed.),. Solubility Data Series, v. 26, p. 187-237. Pergamon Press, Oxford.

Malghe, Y.S. and Kumar, A., 1998. Solubility of CaSO3 in aqueous sucrose solutions from 288 to 368 K. Indian Journal of Chemistry, Section A, v. 37A(1), p. 56-58.

Michalski, J. A., 2000. Sulfur dioxide aqueous solubility in aqueous solutions of calcium or magnesium sulfites. Chem. Eng. Technol., v. 23(6), p.521-525.

Nilsson, G., Rengamo, T. and Sillen. L.G., 1958. Solution equilibriums involving calcium sulfite and carbonate. I. Simple solubility equilibrium of CO2, SO2, CaCO3, and CaSO4. Acta Chemica Scandinavica, v. 12, p. 868-872.

Nordstrom, D.K., 1982. The effect of sulfate on aluminum concentrations in natural waters: some stability relations in the system Al2O3-SO3-H2O at 298 K. Geochim. et Cosomochim. Acta, v. 46, p. 681-682.

Otuka, Y., 1939. Sulfite pulp cooking liquors. I. The vapor pressures at high temperatures of pure sulfurous acid and its binary solutions with a salt of bisulfite. [In Japanese] Kogyo Kagaku Zasshi, v. 42, Suppl. Binding, p. 205-207.

Otuka, Y., 1939. Sulfite pulp cooking liquors. II. The crystallization temperature of calcium sulfite binary solutions of sulfurous acid and calcium bisulfite with and without wood powder and chips. [In Japanese] Kogyo Kagaku Zasshi, v. 42, p. 207-209.

Pokrovskii, V.A., and Helgeson, H.C., 1995, Thermodynamic properties of aqueous species and the solubilities of minerals at high pressures and temperatures: The system Al2O3-H2O-HCl: Amer. Jour. Sci., v. 295, p. 1255-1342.

Rai, D., Felmy, A.R., Fulton, R.W. and Moore, D.A., 1991. An aqueous thermodynamic model for Ca2+-SO32- ion interactions and the solubility of $CaSO_3.1/2H_2O$. Journal of Solution Chemistry, v. 20(6), p. 623-632.

Rempel, S.I., Ryabinina, A.F. and Oshman, V.A., 1974. Kinetics and mechanism of the thermal decomposition of solutions of sulfur dioxide and bisulfites [in Russian]. Ural. Lesotekh. Inst., Sverdovsk. Deposited document, 31 p. CA 86-128024.

Rengamo, T. Brune U. and Sillen. L.G., 1958. Solution equilibriums involving calcium sulfite and carbonate. II. Equilibrium between calcium sulfate and calcium sulfite in aqueous solutions. Acta Chemica Scandinavica, v. 12, p. 873-877.

Rodin, I.V. and Margules, E.V., 1983. Solubility of barium and strontium sulfites in water. Russian Journal of Inorganic Chemistry, v. 28(1), p. 142.

Rodin, I.V. and Margules, E.V., 1983. Solubility of magnesium, calcium and manganese sulfites in water. Russian Journal of Inorganic Chemistry, v. 28(1), p. 144.

Rosenbauer, R.J., Koksalan, T. and Palandri, J,L., 2005. Experimental investigation of CO2–brine–rock interactions at elevated temperature and pressure: Implications for CO2 sequestration in deep-saline aquifers, Fuel Processing Technology, In press.

Ryabinina, A.F. and Oshman, V.A., 1972. Thermal decomposition of aqueous sulfur dioxide solutions. Tr. Ural. Lesotekh. Inst., No. 28, p. 182-189 [in Russian]. CA 79:58115.

Schwartz, R, and Muller-Clemm, H., 1921. Zur kenntnis der sulfitlauge. Zeitschreift fur Angewandte Chemie, v. 34, p. 272-275.

Setoyama, K. and Takahashi, S., 1978. Solid solution of calcium sulfate dihydrate and sulfite hemihydrate [In Japanese]. Yogyo Kyokaishi v. 86(5), p. 133-137.

Setoyama, K. and Takahashi, S., 1979. Solid solution of calcium sulfate dihydrate and sulfite hemihydrate. Part 2. [In Japanese]. Sekko to Sekkai, v. 161, p. 244-250.

Shock, E.L., Sassani, D.C., Willis, M. and Sverjensky, D.A., 1997, Inorganic species in geologic fluids: Correlations among standard molal thermodynamic properties of aqueous ions and hydroxide complexes: Geochim. Cosmochim. Acta, v. 59(21), p. 4329-4350.

Singh, S.S. and Brydon, J.E., 1969. Solubility of basic aluminum sulfates at equilibrium in solution and in the presence of montmorillonite. Soil Science, v. 107(1), p. 12-16.

Tagirov, B. and Schott, J., 2001. Aluminum speciation in crustal fluids revisited. Geochim. Cosmochim. Acta, v. 65(21), p. 3965-3992.

Tai, C.Y. and Chen, P.-C., 1995. Crystal growth of calcium sulfite hemihydrate crystals. Industrial & Engineering Chemistry Research, v. 34(4), p. 1342-1351.

Takahashi, S. and Setoyama, K., 1982. Solid solution of calcium sulfate dihydrate and sulfite hemihydrate. 3. Effect of pH and metal ions on the formation of the solid solution of calcium sulfate dihydrate and sulfite hemihydrate [In Japanese]. Gypsum & Lime, v. 181, p. 290-294.

Templeton, C.C., Rushing, S.S. and Rodgers, J.C., 1963. Solubility factors accompanying oxygen scavenging with sulfite in oil filed brines. Materials Protection, v. 2(8), p. 42-44; 46-47.

Tseng, C.-H.P., 1984. Calcium-sulfite hemihydrate dissolution and crystallization (flue gas, desulfurization), Ph.D Thesis, University of Texas at Austin, 154 p.

Tseng, C.-H.P., and Rochelle, G.T., 1986. Calcium-sulfite hemihydrate: Crystallization growth rate and crystal habit. Environmental Progress, v. 5, p. 5-11.

Zangen, M. and Cohen, A., 1985. Studies on alkaline earth sulfites – VI. Thermal dehydration of $Ca(SO_3)_x(SO_4)_{1-x}.4H2O$. Thermochimica Acta, v. 85, p. 107-110.